energies

MDPI

Article

Real-Time Minimization of Mechanical Specific Energy with Multivariable Extremum Seeking

Magnus Nystad [1,*], Bernt Sigve Aadnøy [1,2] and Alexey Pavlov [1]

[1] Department of Geoscience and Petroleum, Norwegian University of Science and Technology, 7034 Trondheim, Norway; bernt.s.aadnoy@ntnu.no or bernt.aadnoy@uis.no (B.S.A.); alexey.pavlov@ntnu.no (A.P.)
[2] Department of Energy and Petroleum Engineering, University of Stavanger, 4021 Stavanger, Norway
* Correspondence: magnus.nystad@ntnu.no

Abstract: Drilling more efficiently and with less non-productive time (NPT) is one of the key enablers to reduce field development costs. In this work, we investigate the application of a data-driven optimization method called extremum seeking (ES) to achieve more efficient and safe drilling through automatic real-time minimization of the mechanical specific energy (MSE). The ES algorithm gathers information about the current downhole conditions by performing small tests with the applied weight on bit (WOB) and drill string rotational rate (RPM) while drilling and automatically implements optimization actions based on the test results. The ES method does not require an a priori model of the drilling process and can thus be applied even in instances when sufficiently accurate drilling models are not available. The proposed algorithm can handle various drilling constraints related to drilling dysfunctions and hardware limitations. The algorithm's performance is demonstrated by simulations, where the algorithm successfully finds and maintains the optimal WOB and RPM while adhering to drilling constraints in various settings. The simulations show that the ES method is able to track changes in the optimal WOB and RPM corresponding to changes in the drilled formation. As demonstrated in the simulation scenarios, the overall improvements in rate of penetration (ROP) can be up to 20–170%, depending on the initial guess of the optimal WOB and RPM obtained from e.g., a drill-off test or a potentially inaccurate model. The presented algorithm is supplied with specific design choices and tuning considerations that facilitate its simple and efficient use in drilling applications.

Keywords: real-time drilling optimization; extremum seeking; data-driven optimization; mechanical specific energy; rate of penetration

Citation: Nystad, M.; Aadnøy, B.S.; Pavlov, A. Real-Time Minimization of Mechanical Specific Energy with Multivariable Extremum Seeking. *Energies* **2021**, *14*, 1298. https://doi.org/10.3390/en14051298

Academic Editor: Catalin Teodoriu

Received: 18 January 2021
Accepted: 22 February 2021
Published: 26 February 2021

1. Introduction

Drilling a petroleum well is a complicated process with a multitude of factors that affect the drilling efficiency. Because of the high costs associated with well construction, the industry has for more than a century sought to improve drilling performance, in particular through automation and mechanization; a process which has been traced by Eustes [1]. The current state of drilling automation mainly consists of separate functionalities that can aid the driller by performing tasks like providing envelope control [2,3], fault detection [4,5], vibration mitigation [6,7] or selection of the best suited weight on bit (WOB) and drill string rotational rate (RPM) for rate of penetration (ROP) optimization [8,9]. The focus of this study is on developing an automatic system for real-time drilling optimization that automatically seeks out and maintains the WOB and RPM resulting in optimal and safe drilling for the current downhole conditions.

To apply any automated algorithm to drill more efficiently, an objective function is needed to quantify what is meant by optimal drilling conditions. In this work, we employ the mechanical specific energy (MSE) as the objective function to be minimized. The MSE is a measure of the energy required to excavate a unit volume of rock and can

be expressed as a ratio between the rate of energy usage to the rate of penetration [10], which provides a relative measure of the drilling efficiency [11]. The MSE is strongly dependent on the relationship between the ROP and the applied WOB and RPM. It is expected that for a certain region of WOB and RPM values, the bit will drill at peak efficiency [12]. Increasing the WOB or RPM inside the efficient drilling region will result in corresponding proportional gains in the ROP, while the MSE decreases or stays constant. At some threshold value, often referred to as the *founder point*, further increases in WOB or RPM will no longer yield a proportional response in ROP. The lower than expected response in ROP is caused by a drilling dysfunction such as vibrations, bit- or bottomhole balling, which reduces the drilling efficiency and drastically increases the MSE. The founder point can therefore be identified as the combination of WOB and RPM that corresponds to the minimum MSE. If there is no specific operating point that results in minimal MSE, but rather a range of WOB and RPM values at which the MSE is minimal and nearly constant, the founder point can be identified by increasing the WOB and RPM until the MSE starts to grow [12].

It is important to note that drilling at the founder point results in high ROP and the most energy-efficient drilling, but moderately higher ROP can in most cases be obtained by increasing the WOB and/or RPM somewhat past the point of founder. Drilling with dysfunctions can however be deleterious for the bit, downhole tools and borehole quality [12,13], which can result in equipment wear and NPT by having to pull the bit prematurely [14]. The ROP that is achieved when the MSE is at its minimal value is therefore the maximal "good ROP" that can be attained without re-engineering drilling equipment or procedures [11].

In addition to drilling dysfunctions that should be avoided, there are also process constraints that the driller or an algorithm controlling the drilling must adhere to. Drilling at the founder point might not be feasible because of process constraints such as a maximal allowable ROP related to hole cleaning, an upper limit on the WOB to prevent bit damage or top-side energy constraints. In these constrained cases, the authors consider the optimal drilling conditions to be at the smallest MSE value that can be attained without violating the process constraints.

Selecting the optimal WOB and RPM is not a trivial task. Available drilling models might not be accurate enough in predicting the relationship between the ROP and related drilling parameters [15,16]. Varying downhole conditions such as changes in pore pressure or formation properties as well as degradation of the bit teeth/cutters can alter drilling efficiency so that the combination of WOB and RPM that was optimal a short time ago might no longer be the best solution. Historically, designated testing procedures like the Drill-off test [12] or five-point test [17] have been used to empirically explore how the ROP responds to various combinations of WOB and RPM. The downside of this type of "one-time testing" is that the results are only valid for the current downhole conditions, and as soon as the conditions change, the test will have to be repeated.

An alternative to optimization based on models and on "one-time testing" are approaches employing "testing on the fly". In these approaches, the relation between the WOB and/or RPM and an objective function such as the ROP or MSE is explored by performing tests while drilling ahead and selecting more optimal WOB and RPM based on the obtained information. As the downhole conditions change, the repeated tests can identify how the WOB and RPM should be adjusted to drill more efficiently, given the new circumstances. Rommetveit et al. [18] describe an approach of making changes in the WOB and RPM to gather information on how the ROP reacts to these changes. The gathered information can then be used to generate recommendations for the driller or for closed loop control by an optimization algorithm [18]. An automated golden search algorithm that varies the WOB to identify drilling with minimal MSE has been tested on a lab-scale drilling rig [19]. Field trials of advisory systems that can suggest variations in the applied WOB and RPM to search for the drilling conditions that yield the lowest MSE have been described in [20,21]. In recent years, several authors have investigated a data-driven

method called extremum seeking (ES) for drilling optimization. This method relies on continuous testing and optimization based on the test results. Banks [22] explored single variable ES to minimize the MSE with a laboratory drill rig. Aarsnes et al. [23] showed with simulations that ES can be used to seek out the optimal WOB to drill with. A method for adhering to process constraints while optimizing the applied WOB with ES has also been investigated [24]. A drilling optimization system that employs multivariable ES has been tested in the field with good results [25], although no specific details on the algorithm have been provided in that paper.

Extremum seeking is a model-free control algorithm that provides a framework for automatically conducting small tests of the current operating conditions and adapting to the results of the tests to optimize the process. ES has previously been utilized in a variety of engineering systems; an extensive list is provided by Tan et al. [26]. In the context of drilling optimization, the ES algorithm can be employed to find the combination of WOB and RPM which minimizes the MSE (or some other objective function). While drilling ahead, small periodic variations in the WOB and RPM are automatically implemented by the algorithm to test the current drilling conditions. How the MSE responds to these variations is calculated and logged from real-time measurements of the relevant drilling parameters. This generates a local linear "map" of how the MSE is related to the WOB and RPM, which is used by the ES algorithm to make small adjustments in the WOB and RPM in the direction that lowers the MSE. By iteratively performing this procedure of testing and adapting to the results, the WOB and RPM will be steered to the values which result in drilling with minimal MSE. As new tests are performed and new data is recorded, older measurements are discarded from the analysis so that the information used by the algorithm is up to date and representative of the current downhole conditions. In this way, the algorithm will be able to adapt to downhole changes like drilling into a new formation where new values of WOB and RPM might be more beneficial to drill with.

The main advantage of applying the ES method for drilling optimization is that it is model-free, and therefore requires limited a-priori knowledge about the current drilling environment to be employed. When using models to predict how to drill optimally [8,9,15,16,27], the models need to be tuned based on data that is representative of the current downhole conditions. When the conditions change, the models will no longer be valid before they are re-tuned to the new circumstances, which can limit their applicability for real-time optimization. Nevertheless, the drilling models are still a valuable tool that can be combined with data-driven approaches such as Extremum Seeking. The models can provide an initial estimate of the optimal WOB and RPM to drill with, which the ES method can use as a starting point to further improve the drilling efficiency.

In this paper, we present a multivariable ES algorithm that automatically adjusts the WOB and RPM to reach drilling with a minimal MSE value. Although an application of multivariable ES to drilling was presented in [25] with successful field trials, limited details of the algorithm were provided. The algorithm presented in our paper is given in detail with a description of specific design choices and tuning considerations that lead to its simple and efficient use for drilling applications. In addition to that, the presented algorithm can automatically handle operational constraints relevant to safe drilling. The paper details several options on how this functionality can be implemented. Finally, to test the algorithm, a new qualitative model that links the ROP, WOB, RPM and Torque as well as drilling dysfunctions is presented. Without dysfunctions, the model coincides with the drilling model developed by Detournay et al. [28]. This combined model is qualitative when it comes to modelling the dysfunction effects. Yet, it represents phenomena observed in field operations where drilling with dysfunctions result in reduced ROP and high MSE [12–14], and can be utilized for testing of ES algorithms as well as other data-driven (model-free) drilling optimization approaches.

The remainder of the paper is organized in the following way: in Section 2, we formulate the challenge of achieving safe and efficient drilling as an optimization problem and present models that qualitatively describe the relations between the drilling efficiency

in terms of MSE, drilling dysfunctions and operational constraints. These models will be used for testing the proposed algorithm in a simulation environment. In Section 3, the multivariable extremum seeking method and different techniques for constraint handling are detailed together with practical aspects on how to apply and tune the algorithm. Section 4 presents simulation results that demonstrate the performance of the proposed algorithm and highlight its properties. Section 5 contains a discussion of the results of the study, while Section 6 presents conclusions and directions for further work.

2. Safe and Efficient Drilling as an Optimization Problem

The overall goal in drilling optimization (when it comes to mechanical aspects of drilling) is to ensure *WOB* and *RPM* that result in drilling that is both safe for the on-site personnel and drilling equipment (including wear minimization) and provides high efficiency. To achieve this goal, the concept of *MSE* can be used as a performance index to identify the most efficient drilling conditions, which will generate high *ROP* without exposing the bit and downhole tools to excessive vibrations. The latter can accelerate equipment wear and reduce the *ROP*.

Although it is theoretically possible to develop accurate models describing both the rock cutting process and various dysfunctions (e.g., using bit-rock interaction models [28] and advanced proprietary drill string models [14]), such models can be of limited value for real-time drilling optimization. They require detailed knowledge of downhole conditions like mechanical rock properties, the current bit wear state and formation characteristics such as heterogeneity, anisotropy and interbedding [14,28], parameters that change over time and are hard, if possible at all, to measure while drilling. Field experience do however show that at certain combinations of *WOB* and *RPM*, downhole vibrations that can be detrimental to the *ROP* and drilling equipment do occur [9,14,29]. Situations where the drilling efficiency is hampered by vibrations should therefore be accounted for in any optimization approach that attempts to seek out the optimal *WOB* and *RPM* to drill with.

To study drilling optimization in the presence of vibrational effects, we have chosen an approach which qualitatively includes vibrational dysfunctions into a drilling model for polycrystalline diamond compact (PDC) bits [28], and refer to this combined model as the *extended model*. The extended model accounts for vibrations by reducing the *ROP* and thus the drilling efficiency when drilling with combinations of *WOB* and *RPM* that places the operation in regions with expected vibrations. The extended model is qualitative when it comes to modelling the dysfunction effects. Yet, it represents phenomena observed in field operations where drilling with dysfunctions result in reduced *ROP* and high *MSE* [12–14]. When applying static models to replicate the bit/rock interaction, as is commonly done in the literature [28,30], the model variables such as the *WOB*, *RPM* and *ROP* need to be averaged over a suitable time-window for the model to be representative [28]. The same logic is applied in the extended model; it will not capture the dynamics of the dysfunction effects, but it will on average qualitatively represent drilling responses that could be seen in field operations. Because the underlying drilling model [28] in the extended model is defined for PDC bits, we focus on vibrational dysfunction effects, which tend to dominate bit dysfunction with PDC bits [12]. Yet, the extended model could be applied to qualitatively account for other types of dysfunction such as bit- and bottomhole balling as well.

2.1. Drilling Model

The drilling model developed by Detournay et al. [28] is used in this work as a base case scenario to simulate the drilling response of a PDC bit operating under ideal conditions. What is meant here by ideal conditions is that the drilling response for a given bit and formation is fully determined by the interface laws proposed by Detournay et al. [28], which define static relationships between the *WOB*, *RPM*, *ROP* and the bit torque (T) based on bit and formation properties. Drilling dysfunctions such as vibrations are however not covered by this drilling model and will be introduced in the next section. The Detournay

model relies on the existence of three distinct drilling regimes that relate the amount of applied *WOB* and the resulting *ROP* (for a given *RPM*), separated into

- *Phase I drilling*, where the *WOB* is not adequate to force the cutters to fully engage the formation, resulting in inefficient drilling. It is postulated that this inefficiency is caused by the cutters having a blunt underside, a *wear flat*, which supports some of the WOB and is a source of friction that does not contribute to the excavation of rock. In phase I, drilling with higher *WOB* will increase the depth of cut, which translates to higher *ROP*. At the same time, the increased depth of cut will expose a larger area of the wear flats to contact with the formation, which in turn makes the wear flats carry more *WOB*. The *WOB* being translated partly to increased cutting action and partly as friction on the wear flats continues until a threshold *WOB* which marks the onset of the next drilling phase. An ideally sharp bit will in theory never drill in phase I, as it has no wear flats.
- *Phase II drilling*, which is characterized by efficient drilling with the bit acting incrementally as an ideally sharp bit. At the onset of phase II drilling the contact forces between the wear flat and the formation are fully engaged. Further increases in *WOB* value will result in the rock deforming beneath the cutters without any increase in the contact area between the wear flat and formation. An increase in *WOB* while in phase II will be transferred solely to increasing depth of cut and correspondingly increasing *ROP* at peak efficiency, up to a point where a drilling dysfunction starts diminishing the efficiency of the cutting action.
- *Phase III drilling*, where an increase in contact forces between the bit and formation results in less of the applied *WOB* being translated to cutting action, which leads to a reduction in depth of cut and less efficient drilling. The onset of phase III drilling is referred to as the founder point and is often considered the optimal conditions to drill at [12,31].

The relationship between the applied *WOB* and *RPM* and the resulting bit torque (T) and *ROP* in phase I and phase II drilling can be expressed as [28]:

$$ROP(WOB, RPM) = \begin{cases} \frac{c_1 \cdot WOB \cdot RPM}{r}, & WOB \leq WOB_* \\ \frac{c_2 \cdot (WOB - WOB_*) \cdot RPM}{r} + ROP_*, & WOB > WOB_* \end{cases}, \quad (1)$$

$$T(WOB) = \begin{cases} c_3 \cdot r \cdot WOB, & WOB \leq WOB_* \\ c_4 \cdot r \cdot (WOB - WOB_*) + T_*, & WOB > WOB_* \end{cases}, \quad (2)$$

where the asterisk subscript signifies the transition point between phase I and phase II drilling, which is determined by bit bluntness and the formation strength. The values of ROP_* and T_* correspond to the *ROP* and torque at a weight on bit of WOB_*. The parameter r is the bit radius, and c_1, c_2, c_3 and c_4 are model parameters dependent on bit and formation properties.

Equation (1) can be viewed as a calculated depth of cut per bit revolution, determined by the model parameters and the applied *WOB*, which is multiplied with the *RPM* to find the equivalent *ROP*. The torque can be observed from Equation (2) to be independent of the *RPM*, as is often assumed in drilling models [32]. The modelled drilling response from Equations (1) and (2) for a relatively sharp 12 $\frac{1}{4}$" diameter PDC bit drilling through a generic formation *A* is shown in Figure 1, where the transition between phase I and phase II drilling occurs at a *WOB* value of approximately 2700 kg. As Equations (1) and (2) do not account for phase III effects, Figure 1 shows drilling at high efficiency throughout the investigated *WOB* and *RPM* interval after the onset of phase II drilling. In real world drilling operations, the *ROP* response to increasing *WOB* and *RPM* will at some point deviate from the ideal phase II drilling, but the *ROP* response in region III is not unique and depends on the loading path [28] as well as the dysfunction which causes the foundering to occur [12,31]. Region III drilling is therefore not explicitly included in the Detournay

drilling model [28]. A qualitative way of including vibrational drilling dysfunctions in the model is proposed in the next section.

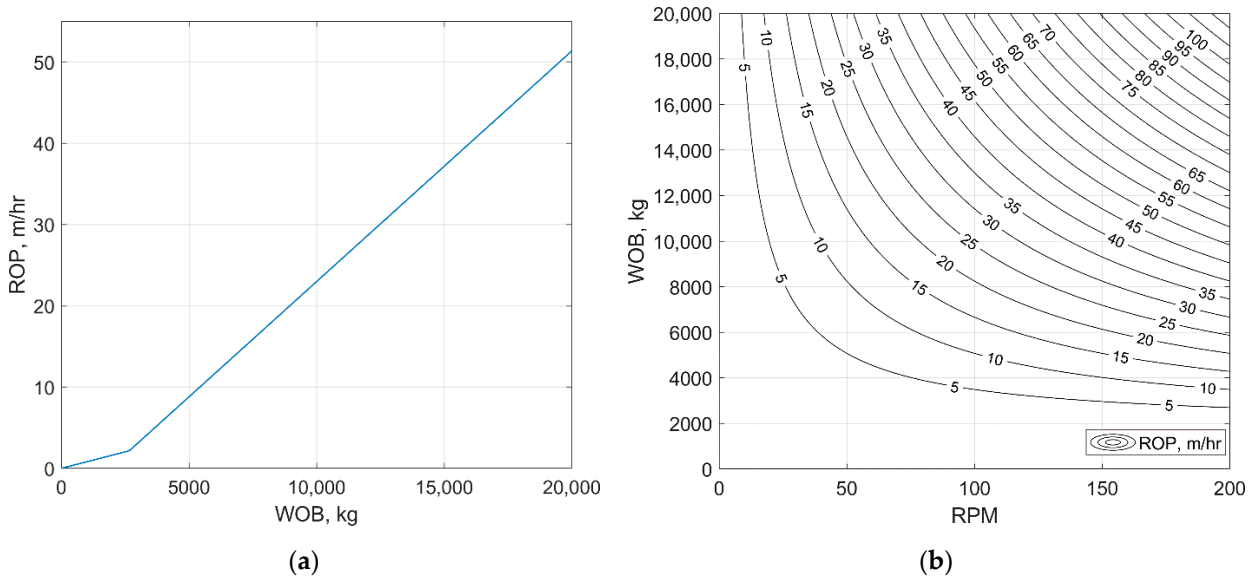

Figure 1. Drilling response in phase I and phase II of the Detournay model [28] for a 12 ¼" bit drilling in the generic formation *A*. (**a**) *ROP* as a function of *WOB* for a constant *RPM* value of 90; (**b**) Contour plot of *ROP* (m/h) as a function of applied *WOB* and *RPM*.

2.2. Drilling Dysfunctions and Constraints

There are a multitude of factors that can affect the drilling efficiency. For an efficient bit drilling with the expected depth of cut, the *ROP* will increase linearly with applied *WOB* or *RPM* as shown in Figure 1, unless a dysfunction reduces the drilling efficiency or a constraint limits the application of additional input energy [12,31]. The factors that influence the *ROP* can in general be grouped into two categories [13]

- *Foundering effects* that reduce the efficiency of energy transferal between the bit and the formation, which causes inefficient drilling. They can be caused by vibrations such as stick-slip and whirl, as well as bit or bottomhole balling. These dysfunctions will result in *ROP* values that are lower than what would be seen with an efficient bit for a given *WOB* and *RPM*.
- *Energy input limiters*, which constrain the amount of energy that can be applied through the input parameters *WOB* and *RPM* when drilling. In the case when the input energy is constrained before the onset of foundering effects, the bit would still be able to drill more efficiently at higher values of *WOB* and/or *RPM*, but because of a system constraint these parameters cannot be increased. A multitude of input energy limiters have been reported in the literature, such as a maximal *WOB* or *RPM* determined by bit or bottom hole assembly (BHA) design, a maximal *ROP* dictated by hole cleaning or solids handling capacity on the surface, a maximal top drive torque rating or top-side vibrations [8,9,13].

The onset of foundering effects and non-bit limiters can in many cases be extended to higher values of *WOB* and *RPM* through reengineering of the drilling equipment [13], but such considerations are beyond the scope of this study. Here, we rather focus on the existence of these effects and how they can be qualitatively included in a drilling model to explore the performance of a data-driven optimization technique in drilling simulation scenarios.

Critical values of *RPM* and *WOB* that trigger the onset of whirl and stick-slip vibrations are heavily affected by bit and BHA characteristics, as well as mechanical rock properties [14]. For an appropriately designed drill string, it is expected that there is a

region of *WOB* and *RPM* which is not notably affected by vibrations, while a combination of high *WOB* and low *RPM* can result in stick-slip vibrations, low *WOB* and high *RPM* can result in forward whirl, and a combination of high *WOB* and high *RPM* can induce backward whirl [9,14,29]. Figure 2 shows the concept of different regions in the *WOB-RPM* plane where the drilling process can be affected by vibrations, together with the *ROP* contours calculated from the Detournay model for formation *A*. The shaded center region in Figure 2 where one would drill with an acceptably high *ROP* while not being affected by the foundering effects was dubbed the *optimum zone* by Wu et al. [14], as it is in this region the combination(s) of *WOB* and *RPM* which results in the most efficient drilling can be found. The locations of the dysfunction regions for formation *A*, as seen in Figure 2, are generically placed in the *WOB-RPM* plane to qualitatively represent a scenario where there is an optimum zone surrounded by regions where dysfunctions will occur [14].

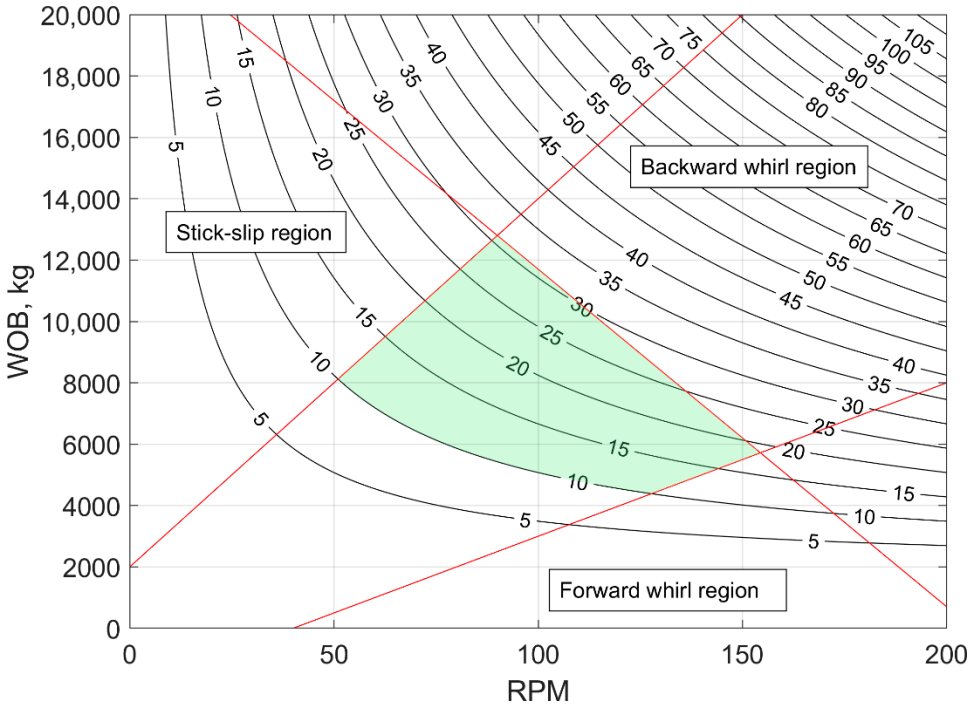

Figure 2. Contour map of dysfunction-free *ROP* (m/h) as a function of *WOB* and *RPM* in formation *A*, with generic critical values of *WOB* and *RPM* which mark the onset of vibrational foundering effects when drilling in this formation.

To incorporate vibrational foundering effects in the drilling model described by Equations (1) and (2) in a qualitative way, a penalty term proposed by the authors is included in the model. The penalty is formulated by defining limits in the *WOB-RPM* plane at which the dysfunctions start to occur, as illustrated in Figure 2. When drilling with a combination of *WOB* and *RPM* that places the operation in a region that is not affected by vibrations, the drilling response is dictated entirely by Equations (1) and (2). When drilling in the regions where vibrations are occurring, the proposed penalty term reduces the *ROP* calculated from Equation (1) by an amount that is dependent on the specific dysfunction and how far into the dysfunction region we are operating. This logic mimics the response seen in field operations for a bit drilling with a dysfunction; if we keep increasing the *WOB* and/or *RPM* further into the dysfunction regions, the experienced *ROP* will deviate further and further away from the straight-line *ROP* response that was expected if the bit was still drilling efficiently [12,13].

In this modified model, which we refer to as the extended model, the torque is not affected by the dysfunctions and is calculated from Equation (2) for all values of *WOB* and *RPM*. This property can be argued for from an *MSE* perspective. In the field, drilling with

vibrational dysfunctions can reduce the drilling efficiency to the extent that the energy consumption at the bit is more than an order of magnitude higher than what the rock strength would indicate [33]. This implies that either the torque continues to grow with the applied *WOB* also in the dysfunction region while the *ROP* is moderately reduced, or that the torque stays constant or decreases while the *ROP* is severely reduced as a response to increasing *WOB*. The former logic is applied in the extended model. Exactly how the torque and *ROP* reacts to drilling with dysfunctions cannot be captured adequately by a static model like the one we are proposing, but the model will be able to qualitatively capture the expected behavior of reduced *ROP* and increased *MSE* when drilling in the dysfunction regions.

The penalty functionality is implemented by means of straight-line functions (as shown in Figure 2) that mark the onset of drilling dysfunctions, but the method we propose is generic and could be applied to other curves as well. The method is in the following explained by an example of drilling with backward whirl, but the same logic applies to the other dysfunctions as well. If we are currently drilling ahead at an *RPM* of 150 and a *WOB* of 11,500 kg, Equation (1) predicts that the resulting *ROP* will be approximately 45 m/h in formation *A*, as can be seen from the contour lines in Figure 2. A penalty for drilling in the whirl region is calculated based on how far into the dysfunction region we are operating, which can be quantified by:

$$L = \sqrt{\left(\frac{WOB - WOB'}{WOB_{max}}\right)^2 + \left(\frac{RPM - RPM'}{RPM_{max}}\right)^2}. \quad (3)$$

In Equation (3), *WOB* and *RPM* are the current operating parameters, *WOB'* and *RPM'* signifies the point on the dysfunction curve closest to the operating parameters, and WOB_{max} and RPM_{max} are normalizing values of 20,000 kg and 200 *RPM*, respectively. The normalization is performed to assign approximately equal weight to the *WOB* and *RPM* when calculating the parameter *L*, which is a normalized measure of how far into the dysfunction region we are operating. When drilling in regions that are not affected by the dysfunctions, the parameter *L* is set equal to zero. Equation (3) is used to find the magnitude of the penalty, *R*, from:

$$R = S(mL) = \begin{cases} 3(mL)^2 - 2(mL)^3, & 0 < mL < 1 \\ 1, & mL \geq 1 \end{cases}, \quad (4)$$

where *S* is the *smoothstep function*, which is a clamping function that gives smooth s-shaped output values between 0 and 1. Using Equation (4) to calculate the penalty, the *ROP* will only be marginally reduced when drilling slightly into any of the dysfunction regions where *L* will take on small values, and more severely affected as *L* grows. The parameter *m* in Equation (4) is a model constant that can be used to customize how much the *ROP* is penalized by the different dysfunctions, so that e.g., whirl can have a stronger negative impact on the *ROP* than stick-slip [12]. In this work, the authors have used generic values of $m = 1$ to calculate the penalty in the forward and backward whirl regions, and $m = 0.5$ for the stick-slip region. When drilling at a point that simultaneously falls within two dysfunction regions, e.g., in the intersection between the stick-slip and backward whirl regions at an *RPM* value of 100 and a *WOB* value of 16,000 kg, the calculated penalty is the sum of the penalties incurred for drilling in both dysfunction regions.

The output *ROP* from the extended model is calculated from:

$$ROP = (1 - R)ROP_D, \quad (5)$$

where the parameter ROP_D signifies the *ROP* calculated from the "ideal" Detournay model in Equation (1), while *R* is calculated from Equations (3) and (4). From Equation (5), the penalized *ROP* that would be output from the model when operating at a *WOB* of 11,500 and an *RPM* of 150 is reduced from 45 to 36 m/h. Figure 3 displays how the *ROP* varies

as a function of *WOB* and *RPM* when the proposed extended model is applied to model drilling in formation *A*. Figure 3a shows a drilling curve for a constant *RPM* value of 90, where it can be observed that *WOB* values above 12,900 kg correspond to drilling with dysfunction, which reduces the *ROP* compared to the straight-line response predicted by the Detournay model. At even higher values of *WOB*, the penalty is further increased and the *ROP* starts decreasing. In Figure 3b, it can be seen from the *ROP* contours produced by the extended model that drilling in the dysfunction regions reduces the *ROP* so that the highest *ROP* that can be achieved in this formation is approximately 38 m/h, which occurs in the region around a *WOB* value of 14,000 kg and an *RPM* value of 120. This maximal *ROP* value does however correspond to drilling somewhat into the backward whirl region (as can be seen from Figure 2), and it does not necessarily represent the optimal conditions to drill at, as will be explained in the next section.

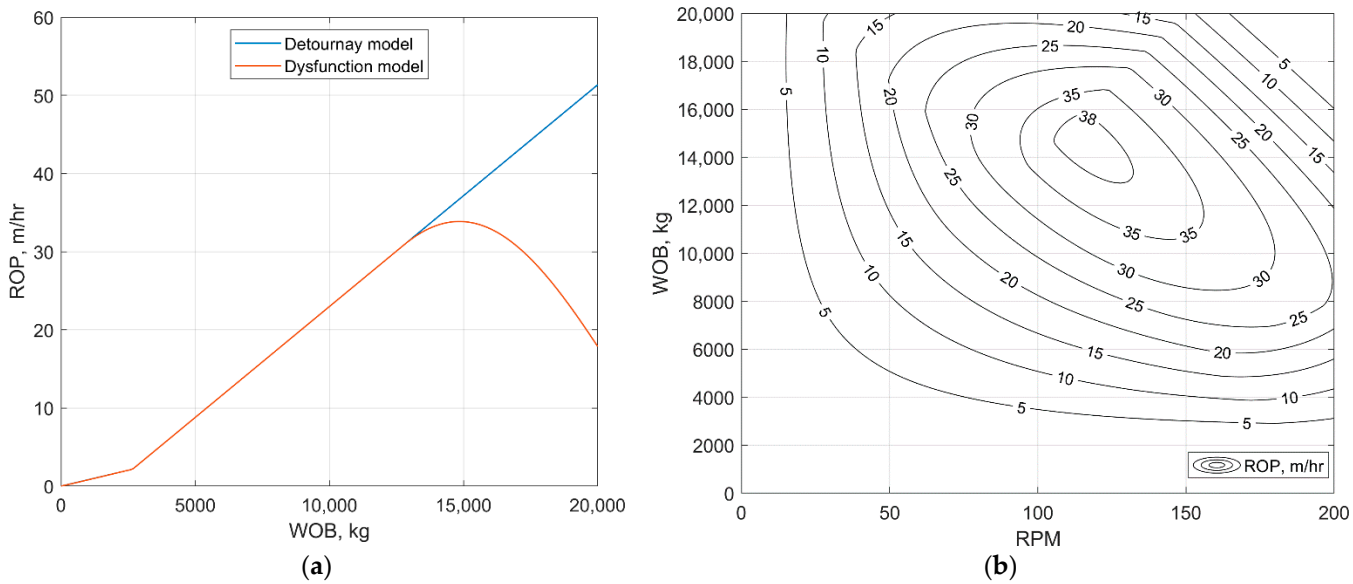

Figure 3. Drilling response with the drilling model including dysfunctions in formation *A*. (**a**) Drill-off curve for a constant *RPM* value of 90; (**b**) Contour plot of *ROP* (m/h) as a function of *WOB* and *RPM* with the extended model.

2.3. Mechanical Specific Energy

The concept of mechanical specific energy (*MSE*) was investigated by Simon [34] and Teale [10] in the sixties and has since been used for applications such as drilling optimization [11,13] and lithology identification [35]. *MSE* is defined as the energy required to excavate a unit volume of rock, and can be expressed as [10]:

$$MSE = \frac{gWOB}{\pi r^2} + \frac{120RPM \cdot \mathrm{T}}{r^2 ROP}, \quad (6)$$

where g is the gravitational acceleration constant with a value of 9.81 m/s^2. Equation (6) can be seen as the ratio between the energy input to the drilling process and the output *ROP*. This ratio will assume its minimal value when drilling at peak efficiency in the transition between phase II and phase III, with higher *MSE* values when drilling in phases I and III [13]. It can be noted that of the two right-hand terms in Equation (6), the rightmost term will normally be larger by a substantial margin and chiefly dictate the value of the calculated *MSE* [10]. To calculate an *MSE* value that reflects the actual energy expenditure at the bit, the downhole torque should be used when using Equation (6) [11,36]. This is because friction along the drill string will cause the surface torque to be higher than the torque on bit. When used as a trending tool, the *MSE* calculated from the surface torque can still be applied to identify more efficient drilling, but with the risk of possible inaccuracies in the analysis caused by fluctuations in the drill string frictional losses. The authors have

assumed in this work that we have access to the downhole torque values, which could come from either measurements from a downhole tool or be calculated from the topside torque with a torque and drag model.

Figure 4 illustrates how the *MSE* varies with *WOB* in formation *A* together with the corresponding drill-off curve. The plot is generated using the extended model detailed in Equations (1)–(5) and a constant *RPM* value of 90. From Figure 4, it can be seen that the minimum *MSE* occurs at a value of approximately 12,900 kg of *WOB*, at the founder point at which the *ROP* starts deviating from straight-line phase II drilling. Higher values of *ROP* can be achieved by increasing the *WOB* past the founder point, but this increase will come at the cost of detrimental foundering effects which can damage the downhole equipment. The minimum *MSE* will therefore correspond to the maximal "good *ROP*" that can be achieved without deleterious side-effects [11]. The shape of the *ROP-WOB* curve in region III will determine how rapidly the *MSE* increases when entering this region, but as long as the *ROP* deviates from the efficient phase II drilling, the *MSE* will increase at this point. This property makes the *MSE* a valuable diagnostic tool for drilling optimization; as long as the *MSE* shows an increasing trend in regions I and III (when moving "outward" from region II drilling in either direction), the most efficient drilling can be identified by seeking out the highest *WOB* that does not make the *MSE* increase.

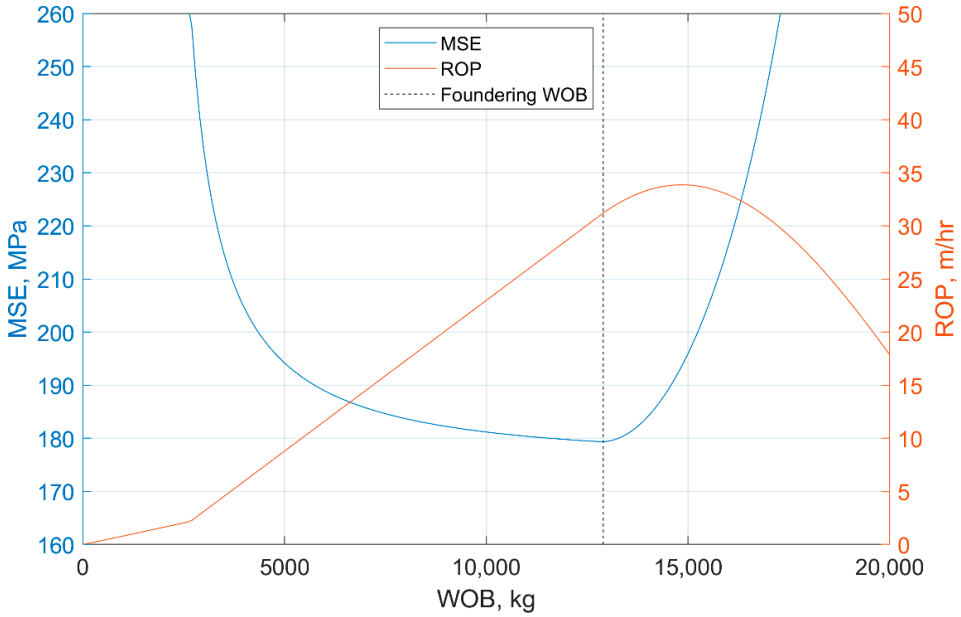

Figure 4. *MSE* and *ROP* as functions of *WOB*, illustrated for a constant *RPM* value of 90.

Figure 5 shows how the *MSE* and *ROP* varies with *RPM* for a constant *WOB* value of 10,000 kg in formation *A*. It can be observed that *RPM* values in the optimum zone, approximately 65 to 115 *RPM*, results in a flat minimum value in the *MSE*. Outside of this region, where dysfunctions affect the drilling efficiency, the *MSE* is seen to increase. This relationship can be deduced from the rightmost term in Equation (6) under the assumption that the *RPM* and torque are not coupled, as is the case with Equation (2). As long as the *ROP* scales linearly with the *RPM*, the *MSE* ratio will remain constant. In the dysfunction regions, where the gain in *ROP* is less than the expected linear relationship with the *RPM*, the numerator in Equation (6) will grow faster than the denominator. The highest *RPM* that can be applied without increasing the *MSE* above the constant minimum value in the optimum region will therefore yield the highest dysfunction-free *ROP* and the most efficient drilling.

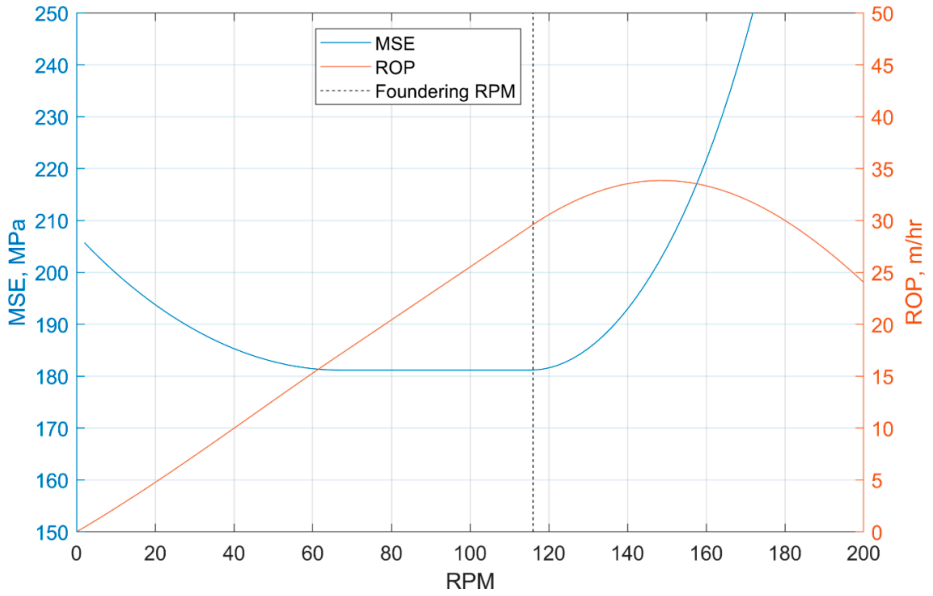

Figure 5. *MSE* and *ROP* as functions of *RPM*, illustrated for a constant *WOB* value of 10,000 kg.

A contour plot detailing how the *MSE* varies as a function of applied *WOB* and *RPM* is shown in Figure 6. This plot is generated using the proposed extended model, where the *ROP* is penalized when drilling in the three dysfunction regions (as shown in Figure 2). As can be seen in Figure 6, there is a region around the point at which the *WOB* value is approximately 12,900 kg and the *RPM* value is 90, where one would drill with the minimal *MSE* value of 180 MPa. This point corresponds to the top corner of the optimum zone depicted in Figure 2. Moving away from this low *MSE* region in any direction will increase the *MSE*; at first with small values and then progressively larger values as we move into the different dysfunction regions where drilling is less efficient. Comparing Figures 6 and 3b, it can also be observed that the highest possible *ROP* values which are found in the region around a *WOB* of 14,000 and an *RPM* of 120, correspond to drilling with a dysfunction, as is reflected by the higher *MSE* values around this point in Figure 6.

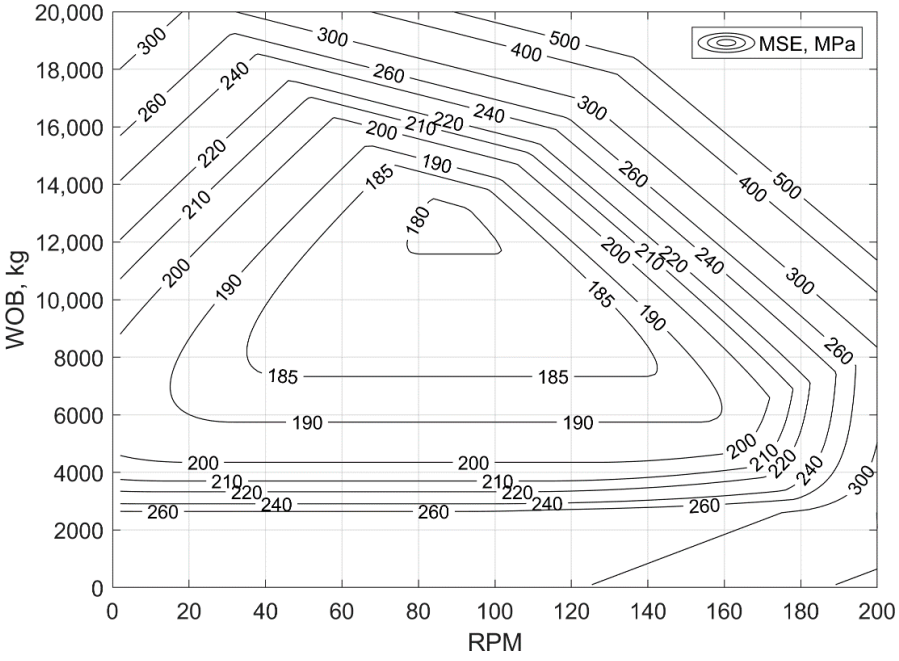

Figure 6. Contour plot of MSE as a function of WOB and RPM in formation *A*.

3. Drilling Optimization with Extremum Seeking

As detailed in Section 2, accurate modelling of the drilling process, which regions will be affected by dysfunctions and which combination(s) of *WOB* and *RPM* which will yield the most efficient drilling is a challenging task. Not knowing at which point drilling dysfunctions will be induced can cause the driller to use conservative limits imposed on the *WOB* and *RPM*, which can result in sub-optimal drilling. Accurate modeling of the drilling process will often require detailed knowledge of downhole parameters which cannot be measured directly and are therefore hard to obtain in real-time operations. The situation is further complicated by changes in downhole conditions which can cause models tuned to data from before the change to no longer be valid for the current circumstances.

Employing a data-driven optimization technique like ES can be used to solve these challenges, as the method does not rely on having detailed a priori knowledge of the downhole conditions. The ES algorithm relies instead on executing small tests while drilling ahead by varying the applied *WOB* and *RPM*. Real-time measurements of how drilling parameters such as the *ROP*, *T* and calculated *MSE* vary when the tests are performed are recorded by the algorithm. The measured response to the tests represents the most up to date knowledge on how the drilling process reacts to changes in *WOB* and *RPM* and are automatically used by the algorithm to perform optimization actions that reduce the *MSE* if possible. When a change in downhole conditions occurs, such as a formation shift, this will be reflected in the measured drilling parameters and the ES algorithm will be able to adapt to the new downhole circumstances.

Using the *MSE* as an objective function to quantify when we are drilling efficiently can be a powerful tool for drilling optimization. If the *MSE* exhibits the general shape shown in Figure 6; where drilling efficiently will result in lower *MSE* values and drilling into the dysfunction regions will make the *MSE* progressively increase, the proposed ES algorithm can be used to seek out the *WOB* and *RPM* that result in drilling with minimal *MSE*. The only a priori information that is needed is knowing the general shape of the *MSE* response to drilling efficiently and inefficiently, as well as some general drilling engineering knowledge that is needed to initiate and tune the algorithm. The ES method is an iterative algorithm, which means that it needs to be initiated when drilling at some *WOB* and *RPM* and use this as a starting point from which it can perform optimization actions. This starting point can be viewed as an "initial guess" of the optimal *WOB* and *RPM*, and can be based on the drillers experience, data from an offset well or an estimate provided by a drilling model.

3.1. The Extremum Seeking Algorithm

Extremum seeking is in essence a hill climbing optimization method that is applied to a process in real-time. ES works by systematically exciting the system to gather information about the current operating conditions by varying one or several controllable input variables. Real-time and recent measurements are used to calculate an objective function that quantifies the system's reaction to the excitations. Based on how the objective function changes with the variations in the input parameters, the ES algorithm will automatically make small changes to the input variables that steers them towards the values optimizing the objective function. This happens in an iterative fashion, where new measurements are continuously included in the analysis and old measurements are discarded. The optimization method does not require a model of the system, since all adjustments are performed based on measurements of how the process performs with different values and combinations of the input variables.

In this work, we consider a multivariable ES approach in which the controllable variables we seek to manipulate to drill more optimally are the *WOB* and *RPM*. The *MSE*, as detailed in Equation (6), is used as an objective function to quantify what combination of *WOB* and *RPM* constitutes optimal drilling. The procedure is illustrated in Figure 7, where the left-hand plot demonstrates how the ES algorithm automatically varies the *WOB* and *RPM* to investigate the drilling response in the local region marked with green shading.

The right-hand tracks show the varying input variables and the resulting *MSE* as functions of time. It can be observed from Figure 7 that, in this case, higher values of both *WOB* and *RPM* results in lower *MSE*, which would prompt the ES algorithm to slowly increase the *WOB* and *RPM*, as indicated by the dotted lines. This procedure of testing and adapting to the *MSE*-response is performed continuously and will over time drive the system to drill at the optimal conditions that minimize the *MSE*. In cases where the *MSE* does not change when the *WOB* and/or *RPM* are varied, this is interpreted by the proposed ES algorithm as a situation where it should increase the applied *WOB* and/or *RPM* further, as explained in Section 2. Several techniques for avoiding violation of drilling constraints are proposed and implemented in the following, to ensure that the ES algorithm will adhere to process limitations while seeking out the minimal *MSE*.

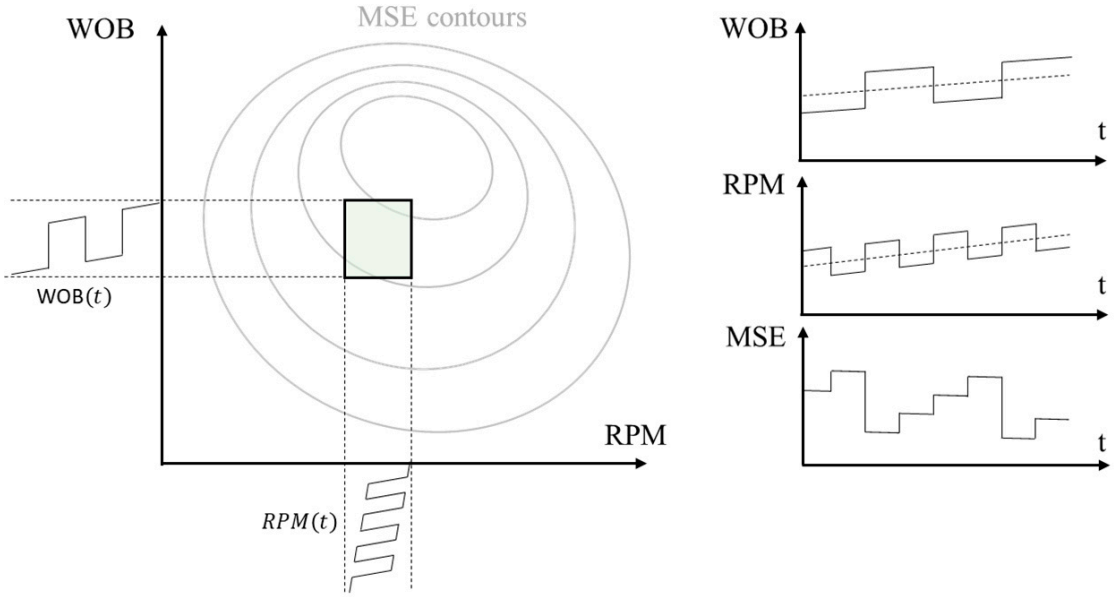

Figure 7. Concept illustration of multivariable ES applied to minimize the MSE.

The ES algorithm can be split into three main components:

- *The excitation signal*, which varies the input variables around a base value to investigate the current drilling conditions.
- *Gradient estimation*, which quantifies how the process reacts to the excitation signal by estimating partial derivatives of the objective function with respect to the input variables.
- *Adaptation*, which adjusts the base values of the input variables with a magnitude and direction determined by the estimated gradients, to seek out drilling conditions that result in lower *MSE* values.

These components are detailed in the subsequent sections. Because the measurements of drilling parameters and commands given to the control system on the rig are performed at regular intervals, discrete time notation is used. It is assumed that relevant measurements are performed at a time interval of Δt seconds, and that the top drive and autodriller can receive updated setpoints for target *RPM* and *WOB* every Δt seconds. For simplicity, Δt is set to a value of 1 s. The current timestep is denoted by t, so that a command for the coming timestep is indicated by the notation $t + \Delta t$.

3.1.1. The Excitation Signal

To probe the current drilling conditions, a periodic excitation signal is continuously applied to the input variables. Assume that we are currently drilling ahead with the base values $\overline{WOB}$ and $\overline{RPM}$ as initial guesses of the optimal input variables. These initial values could be based on e.g., data from an offset well or estimates given by a drilling model.

The ES algorithm dictates a periodic variation in the *WOB* and *RPM* about the base values according to:

$$WOB(t) = \overline{WOB}(t) + d(t, A_{wob}, P_{wob}), \tag{7a}$$

$$RPM(t) = \overline{RPM}(t) + d\left(t, A_{rpm}, P_{rpm}\right), \tag{7b}$$

where the left-hand sides signify the *WOB* and *RPM* that will be sent to the control system on the rig as setpoints. The parameters A and P are the amplitude and period of the excitation signal, d, which is given by:

$$d(t, A, P) = A \cdot \text{sgn}\left(sin\left(\frac{2\pi t}{P}\right)\right). \tag{8}$$

Equation (8) describes a square wave, where *sgn* is the *signum function* which takes a value of 1 when the argument is positive, a value of 0 when the argument is zero and a value of -1 when the argument is negative. The applied *WOB* and *RPM* prescribed by Equations (7a) and (7b) will oscillate about the base values, $\overline{WOB}$ and $\overline{RPM}$, with amplitudes of $\pm\, A_{wob}$ kg and $\pm\, A_{rpm}$ rpm, respectively. Through the information gathered from the excitation signals, the ES algorithm will adjust the base values in the direction that reduces the *MSE*.

The induced variations in *RPM* and *WOB* can potentially influence the measured *MSE* to different extents and in different directions. For the ES algorithm to be able to draw conclusions as to how the two input variables individually affect the drilling efficiency, the parameters P_{wob} and P_{rpm} should be designed to minimize the coupling between the *MSE*-responses resulting from the two signals. In this work, the periods of the excitation signals are set so that $P_{wob} = 2P_{rpm}$. This tuning is illustrated in the right-hand tracks in Figure 7, where the *RPM* oscillates with twice the frequency of the *WOB*-signal. For each half-period of the *WOB* fluctuations, the *WOB* remains relatively constant while the *RPM* performs a full oscillation, from which the dependency between the *MSE* and *RPM* can be deduced by the gradient estimator. The frequency of the *RPM* signal is an even multiple of the *WOB* signal frequency, causing the average *RPM* value during each period of the *WOB* oscillation to be approximately $\overline{RPM}$. This allows for estimation of the relationship between the *MSE* and the varying *WOB* as if the *RPM* was held constant. The tuning of the excitation signals is further explored in Appendix A.

3.1.2. Gradient Estimation

To estimate a local model of the *MSE* as a function of the applied *WOB* and *RPM*, a lest-squares approach is used in this work. As we drill ahead, measurements of the *WOB*, *RPM*, *T* and *ROP* as well as the calculated *MSE* are stored in buffers containing a few minutes of the most recent data. These buffers contain a sliding window time series of data that represents the most up to date information that is available about the current drilling conditions. At each update of measurements, the newest measurements are included in the buffers, while the oldest are discarded. The buffers contain data from one period of the excitation signal with the longest period time, which in this case is P_{wob} seconds.

The excitation signals are designed to elicit responses in *MSE* that can be associated with each individual signal. This allows the gradient estimation to be performed by correlating the variations in measured *MSE* with the applied *WOB* and *RPM*. At each new timestep, Δt, the updated buffers are used to solve the least-squares problem:

$$\sum_{i=0}^{P_{wob}-1} \left(MSE(t - i\Delta t) - \left(a_{wob}WOB(t - i\Delta t) + a_{rpm}RPM(t - i\Delta t) + b\right)\right)^2 \rightarrow \min_{a_{wob}\,, a_{rpm},\, b}. \tag{9}$$

In Equation (9), a_{wob}, a_{rpm} and b are the slopes and intercept, respectively, of the lest-squares fit. The parameters a and b represent a linear approximation (local model) of how

the *MSE* correlates with the input variables. The calculated slopes are used as estimates of the partial derivatives of the *MSE* with respect to *WOB* and *RPM* by setting:

$$\left.\frac{\partial MSE}{\partial WOB}\right|_{\overline{WOB}(t),\overline{RPM}(t)} \approx a_{wob}(t), \quad \left.\frac{\partial MSE}{\partial RPM}\right|_{\overline{WOB}(t),\overline{RPM}(t)} \approx a_{rpm}(t). \tag{10}$$

The gradients described by Equation (10) are based on the P_{wob} $\left(=2P_{rpm}\right)$ seconds of the most recent measurements and represent the current best estimate of how the *MSE* is related to the input variables in the local region that has been explored by the excitation signals. Because of the symmetry of the excitation signals, the average values for *WOB* and *RPM* during P_{WOB} seconds of drilling will on average be close or equal to $\overline{WOB}(t)$ and $\overline{RPM}(t)$, respectively, which is why the gradients in Equation (10) are evaluated at this point.

3.1.3. Adaptation

Assuming that there is a response in the *MSE* to the variations in the input variables, the gradients calculated from Equations (9) and (10) determine in which direction the *WOB* and *RPM* should be adjusted to reduce the *MSE*. When drilling in the optimum zone, the changes in *MSE* resulting from variations in the *WOB* and *RPM* are expected to be small. This results in zero or near zero values for the estimated gradients. When using *MSE* to increase real-time performance, a negative or zero gradient value indicates that drilling is efficient and the input *WOB* and/or *RPM* should be increased until the point of foundering [12]. To include this logic in the ES algorithm, a tuning parameter, k, is subtracted from the estimated gradients. This makes the algorithm see a zero gradient as a scenario where the corresponding input should be increased.

From the estimated gradients at the current timestep, the ES algorithm prescribes updated base values for the input variables for the coming timestep from:

$$\overline{WOB}(t+\Delta t) = \overline{WOB}(t) - \gamma_{wob}\cdot\text{sat}\left(\left.\frac{\partial MSE}{\partial WOB}\right|_{\overline{WOB}(t),\overline{RPM}(t)} - k_{wob}, \sigma_{wob}\right)\Delta t, \tag{11a}$$

$$\overline{RPM}(t+\Delta t) = \overline{RPM}(t) - \gamma_{rpm}\cdot\text{sat}\left(\left.\frac{\partial MSE}{\partial RPM}\right|_{\overline{WOB}(t),\overline{RPM}(t)} - k_{rpm}, \sigma_{rpm}\right)\Delta t. \tag{11b}$$

The left-hand sides of Equation (11) denote the new base values that will be used in Equations (7a) and (7b) in the next iteration of the algorithm. It can be observed from Equations (11a) and (11b) that for each iteration, the input base values, $\overline{WOB}$ and $\overline{RPM}$, will change incrementally from their previous values with a magnitude dictated by the rightmost terms. The magnitude of this incremental change is determined by the adaptation gain, γ, and the output of the saturation function, *sat*, which is given by:

$$sat(x,\sigma) = \begin{cases} -1, & x \leq -\sigma \\ x/\sigma, & -\sigma < x < \sigma. \\ 1, & x \geq \sigma \end{cases} \tag{12}$$

The use of Equation (12) in combination with Equation (11b) is illustrated in Figure 8. In Equation (12), σ is a tuning parameter that determines the width of the region where the saturation function shifts from negative to positive output values. The saturation function is used to limit the maximal step size that the ES algorithm is able to implement per iteration by using the principle of sliding mode extremum seeking control [37]. As the maximal output of Equation (12) is a value of ± 1, the greatest rate of change that the algorithm can demand in the input variables is given by γ. This property makes the algorithm easier to tune from a safety standpoint, as the maximal adaptation rate is explicitly stated by the parameter γ in units of kg or rpm per second.

The maximal limit on adaptation rate is useful in cases where an abrupt change in drilling conditions occurs, e.g., a formation change, as the gradients calculated by Equations (9) and (10) can be erroneous in this situation. This error would be introduced by the algorithm's assumption that any changes in the *MSE* can be attributed to the variations in the *WOB* and *RPM*. For a large change in *MSE* caused by differences in lithology, the estimated gradients could become artificially large as the algorithm relates the relatively small *WOB* and *RPM* oscillations to a large change in *MSE*. If the adaptation was directly proportional to the estimated gradients in this scenario (as is done in conventional ES algorithms, see e.g., Tan et al. [26]), it could cause the ES algorithm to demand large and rapid changes in the $\overline{WOB}$ and/or $\overline{RPM}$ that could steer the system away from the optimum and into the dysfunction regions. It should be noted that in a case like this, the estimated gradients would only be erroneous for a brief time window before the buffers would be filled with data representative of the new formation, which would produce more accurate gradient estimates. The downside of limiting the adaptation with Equation (12) is that in cases where the estimated gradients correctly indicate that large improvements in drilling efficiency could be achieved by adapting the inputs, the rate at which the inputs are adapted to more suitable values will be limited. Weighing faster adaptation versus more robust control is an algorithm design and tuning consideration, where the authors have opted to lean towards more robust control through the use of the saturation function.

The saturation function is illustrated in Figure 8, which exemplifies how this function is applied in Equation (11b) for *RPM* optimization. The example parameter values $\sigma_{rpm} = 2$, $k_{rpm} = 1$ and $\gamma_{rpm} = 1$ are used in Figure 8. It can be seen that for a gradient value of zero, the saturation function will yield an output of -0.5, which will translate to an increase of $\gamma_{rpm}/2$ in the base value $\overline{RPM}$ for the next timestep. When drilling in the optimum zone, the estimated gradient is expected to have a low or zero value, and the proposed ES algorithm relies on the parameter k_{rpm} to indicate that the *RPM* should be increased to reach the foundering point, see Section 2.3. With this configuration, the algorithm will request increasing *RPM* until the estimated gradient is equal to k_{rpm} in magnitude and the saturation function's output is zero. At some point, the ES algorithm will drive the value of $\overline{RPM}$ close to the dysfunction region. Because the *MSE* is expected to increase drastically when drilling dysfunctions occur [13], the gradients estimated past this point will take on relatively large, positive values. A suitably small value of k_{rpm} will therefore provide increasing $\overline{RPM}$ values up to the limit at which foundering starts to occur. If, for some reason, drilling outside of the optimal region occurred, the large estimated gradients would make the ES algorithm adapt at its maximal rate of γ_{rpm} rpm/s to exit the dysfunction region as quickly as possible. The same logic as described above also applies to the adaptation in *WOB* determined by Equation (11a).

A block diagram of the proposed ES algorithm is shown in Figure 9. A loop through this diagram represents an iteration of the ES algorithm, which is continuously repeated every Δt seconds. Starting from the lower left corner, the updated base values and excitation signal values are combined to produce new values for the *WOB* and *RPM*, which are fed as setpoints to the control system on the rig. The resulting *ROP*, torque, *WOB* and *RPM* values are measured and used to calculate the current *MSE* value. The new measurements are subsequently included in the buffers, while the oldest measurements are discarded. The updated buffers are used to estimate the current gradient values, which are translated to updated base values that are employed in the next iteration of the algorithm.

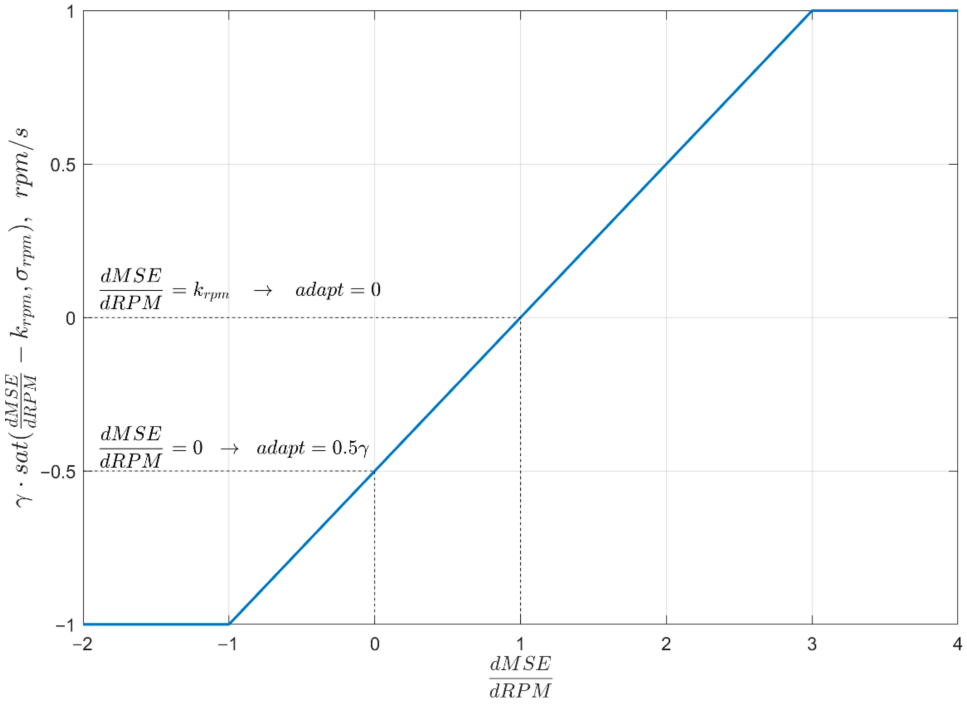

Figure 8. Illustration of the saturation function and how it is applied in Equation (11b), with the example parameter values $\sigma_{rpm} = 2$, $k_{rpm} = 1$ and $\gamma_{rpm} = 1$.

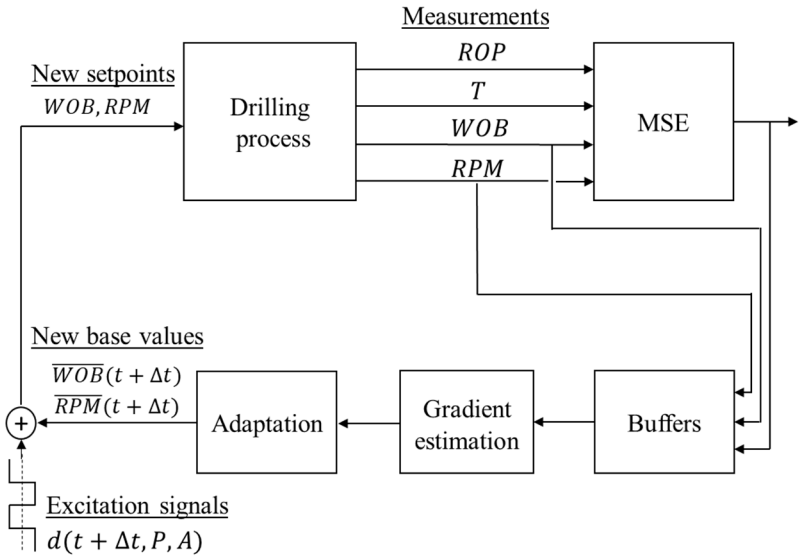

Figure 9. Block diagram of multivariable extremum seeking applied to minimize the *MSE*.

3.2. Algorithm Design Choices

The Extremum Seeking method provides a whole range of algorithms and tools suitable for various applications, starting with the fundamental ES controllers described in [26,38]. The ES algorithm presented in this paper is a result of selection various elements from this toolbox to make it robust and well suited for drilling applications.

In particular, the square wave excitation signal was chosen because this is the signal shape that, for a given amplitude, gives the maximal (output) signal power and results in faster convergence to the optimal values at least for the standard ES algorithm configurations [39]. It is also expected that square excitation waves are more suitable for realizing *WOB* variations with a standard autodriller functionality.

We can expect that due to transients and various disturbances acting on the drill string, the actual *WOB* and *RPM* realized by the autodriller and top drive may noticeably deviate from the corresponding setpoints requested by the ES algorithm. Gradient estimation by the selected least-squares method is less affected by these deviations. In addition to this, the selected gradient estimation technique accounts for changes in $\overline{WOB}$ and $\overline{RPM}$ (caused by adaptation) and will therefore calculate more accurate gradients than the standard ES method.

Finally, we have opted to use the saturation function in the adaptation block defined in Equation (11), to limit the rate of change for $\overline{WOB}$ and $\overline{RPM}$. This makes the algorithm more robust when experiencing sudden changes in downhole conditions, e.g., a formation shift.

3.3. Constraint Handling

The ES algorithm detailed in the previous section will automatically steer the *WOB* and *RPM* towards the optimal values that minimize the *MSE*. As the *MSE* will increase greatly when foundering occurs, the ES algorithm will inherently try and avoid these dysfunctions by seeking out dysfunction-free combinations of *WOB* and *RPM*. There are however many situations where drilling at the minimal *MSE* is not feasible, as the drilling process is restricted by energy input limiters, as described in Section 2.2. It is imperative that the ES algorithm does not exceed these process constraints in the search for the minimal *MSE*.

A distinction can be made between constraints that are known a priori in the *RPM*-*WOB* plane and constraints related to process output values that are not known in advance. In the former category, a maximal *WOB* associated with e.g., a buckling criterion can be implemented in the algorithm with a logic condition that would not allow for increase in the *WOB* past a certain point, even if the algorithm recognized potential for lower *MSE* at *WOB* which would exceed the buckling criterion. A similar logic condition could enforce e.g., a maximal *RPM* value related to surface vibrations. In the latter category, where e.g., a maximal *ROP* related to hole cleaning should not be exceeded, the combinations of *WOB* and *RPM* that produce too high *ROP* are not known in advance and a different approach is needed. Three techniques that can be used to ensure that the ES algorithm does not violate constraints related to process outputs while searching for the optimum drilling conditions are investigated in the following. The constraint handling techniques are generic and can be applied to different types of limitations. To demonstrate the constraint handling techniques, we apply them to maximal values imposed on the torque and the *ROP* that the ES algorithm must adhere to.

3.3.1. Modified Objective Function

A practical way of making the ES algorithm avoid e.g., *ROP* values above a given threshold, is through modification of the objective function. Instead of trying to minimize the *MSE*, an objective function on the form:

$$J = MSE \cdot \left(1 + \rho \frac{\max(0, ROP - ROP_{threshold})}{ROP_{threshold}}\right) \tag{13}$$

is used in the ES algorithm to identify the optimal combination of *WOB* and *RPM*. A function similar to Equation (13) has previously been explored to limit drilling with stick-slip [40]. In Equation (13), *max* is a function which outputs the largest of the input arguments and ρ is a tuning parameter that determines how much the objective function increases when drilling with higher than allowed *ROP*. The modified objective function, *J*, will start increasing when the threshold *ROP* is exceeded, which will make the ES algorithm avoid higher *ROP* values. Different constraining parameters can be added to Equation (13) in a similar fashion as the *ROP* term, to penalize the presence of e.g., measured vibrations or high torque, making this constraint handling technique very versatile. A downside of this approach is that if e.g., a sudden change in drilling conditions makes the *ROP* increase

by a some margin above the threshold, the time it takes for the ES algorithm to steer the *WOB* and *RPM* to better values is determined by the rather slow adaptation rate dictated by γ. A more prudent approach would then be to use a separate control loop with the ability to modify the applied *WOB* and/or *RPM* more rapidly.

3.3.2. Predictive Constraint Handling

A combination of a predictive and a reactive constraint handling technique that can be used to avoid violation of a constraint related to the torque has been tested in the case of single variable ES [24]. Here, we demonstrate that these techniques can also be applied in a multivariable ES approach. It must be noted that when using the predictive constraint handling technique, it should be combined with the reactive approach, as this ensures that the constraint handling does not make the ES algorithm "get stuck".

The predictive constraint handling method [24] relies on obtaining additional information about the downhole conditions by relating changes in measured output parameters to the known variations of the excitation signals. For this purpose, the same least-squares technique as detailed in Equation (9) can be used to estimate a gradient of how the torque relates to the *WOB*. This technique relies on the assumption that the torque is mainly a function of the *WOB*, as is commonly assumed in the literature [28,32]. Considering a sliding window time series that contains measured values of the torque and *WOB* for the past P_{wob} seconds, a gradient describing the current *T*-*WOB* relationship can be estimated from:

$$\sum_{i=0}^{P_{wob}-1} \left(T(t-i\Delta t) - (\alpha \cdot WOB(t-i\Delta t) + \beta)\right)^2 \rightarrow \min_{\alpha,\,.\beta}, \tag{14}$$

$$\left.\frac{\partial T}{\partial WOB}\right|_{\overline{WOB}(t),\overline{RPM}(t)} \approx \alpha(t). \tag{15}$$

In Equations (14) and (15), α and β are the least-squares slope and intercept, respectively. As the parameter α is a linear fit to how the torque has changed recently as a function of *WOB*, α can be used to predict what the torque will be if the *WOB* is increased or lowered in the region around $\overline{WOB}$. As long as a reasonably accurate estimate of the torque gradient can be obtained, it can be used to stop the *WOB* from being steered to a region where the torque is higher than allowed, assuming that we are operating at a point where the torque constraint is currently not violated.

Let T_{avg} denote the average measured torque value for the past P_{wob} seconds. The torque constraint which we do not want to exceed is represented by T_{limit}. To avoid the *WOB* being steered to values which would cause the torque to grow past the allowable limit, the following rule is imposed on the *WOB* adaptation gain:

$$\gamma_{wob} = \begin{cases} \gamma_{wob}, & \left(T_{B,avg} + A_{wob}\alpha(t)SF\right) < T_{limit} \\ 0\,, & \left(T_{B,avg} + A_{wob}\alpha(t)SF\right) \geq T_{limit} \end{cases}. \tag{16}$$

The rule formulated in Equation (16) takes advantage of the fact that during one oscillation of the excitation signal, the weight on bit will take on values in the range $\overline{WOB}(t) \pm A_{wob}$. Assuming that the adaptation gain is low, the value of $\overline{WOB}$ will be nearly constant in this time interval and the average weight on bit will be approximately equal to $\overline{WOB}$. The average torque value, T_{avg}, will therefore correspond to drilling with a weight on bit of $\overline{WOB}$ kg. The product $A_{wob}\alpha(t)$ is a projection of how much the torque will grow if the *WOB* is increased by a value of A_{wob} kg. This product is multiplied by a safety factor with a value greater than 1, which determines how far away from the torque limit we wish to stop the *WOB* adaptation. Using e.g., a safety factor of 2, Equation (16) will stop the *WOB* adaptation when $\overline{WOB}$ is $2A_{wob}$ kg away from the weight on bit value which would make the torque exceed its limit. Stopping the adaptation with some margin will allow the ES algorithm to continue performing the *WOB* excitations without the torque limitation being violated.

3.3.3. Reactive Constraint Handling

There are instances where Equation (16) will not be adequate to avoid violation of the torque constraint. The torque measurements are commonly very noisy, which can cause the estimated gradient to be inaccurate. Changes in downhole conditions could affect the torque in a way that cannot be predicted by the gradient, causing the torque to exceed its maximal limit. In this case, a reactive constraint handling technique should be used in combination with the predictive method to automatically steer the *WOB* back to the safe region if the torque constraint is violated [24]. At each timestep a variable, e, is calculated that quantifies if the constraint is violated and in which case by how much:

$$e(t) = \begin{cases} 0, \ T(t) < T_{limit} \\ T(t) - T_{limit}, \ T(t) \geq T_{limit} \end{cases}. \tag{17}$$

If the variable e takes on a value larger than 0, this indicates that the constraint is violated and the adaptation gain, γ_{wob} is set to zero. In Equation (17), T is the measured torque value at the current timestep. If the torque measurements are very noisy, the torque used in Equation (17) should be filtered to avoid that the constraint handling reacts too aggressively as a response to noise [24]. The variable e from Equation (17) is used as the error term in a discrete proportional-integral (PI) controller which calculates a penalty, λ, from:

$$\lambda(t) = K_P e(t) + K_I \Psi(t) \Delta t, \tag{18}$$

$$\Psi(t) = \begin{cases} 0, \ T(t) < T_{limit} \\ \sum_{i=n}^{t} e(i), \ T(t) \geq T_{limit} \end{cases}. \tag{19}$$

In Equation (18), K_P and K_I are the proportional and integral gains, respectively. These parameters are used to tune the controller and determine how fast the *WOB* will be adjusted if the torque exceeds the imposed limit. If the torque constraint at some point in time is violated, the summation term, Ψ, will continue to grow and make the penalty term larger until the torque is adjusted down to acceptable levels. At the time when the torque is returned to a level below the limiting value, the summation term is reset by setting the parameter n equal to this time, t, essentially forgetting that the torque constraint has previously been violated and continuing optimization with the ES algorithm from this point on.

The *WOB* that is requested by the ES algorithm is adjusted based on the penalty according to:

$$\overline{WOB}_{constrained}(t + \Delta t) = \overline{WOB}(t + \Delta t) - \lambda(t). \tag{20}$$

The first term on the right-hand side of Equation (20) is the $\overline{WOB}$ value calculated from Equation (11a). The variable $\overline{WOB}_{constrained}$ is used in Equation (7a) as the base *WOB* value when the constraint handling is activated. As long as the torque limit has not been violated, λ will be equal to zero and the WOB will not be adjusted by Equations (17)–(20). The penalty term, λ, will grow if we are drilling with torque values above the allowable limit, which will cause the applied *WOB* to be reduced according to Equation (20) until the torque is within the allowable bounds and λ is reset to a zero value. Making these adjustments to the $\overline{WOB}$ with Equation (20) rather than Equation (13) allows the algorithm to reduce the applied *WOB* faster, which will cause the torque constraint to be violated for a shorter period of time. It can be noted that the reactive constraint handling method will not make any adjustments to the *WOB* until the torque limit is exceeded. For this reason, a lower value for T_{limit} than the actual system's limit should be used in Equations (17) and (19).

3.4. Practical Requirements and Algorithm Tuning

Implementation of the proposed algorithm requires the following measurements: *WOB*, *RPM*, bit torque (either calculated or measured), and calculated *ROP*. These measurements are used to calculate the *MSE* from Equation (6). In essence, the components of

the ES algorithm act like filters when calculating the gradients and performing adaptation of the *WOB* and *RPM* values. Yet, if the measurements are too noisy, appropriate filtering should be applied before using them in the algorithm.

The algorithm automatically adjusts the setpoints for the *WOB* and *RPM*, which are then used by the autodriller to control the actual *WOB* and by the top drive to control the actual *RPM*. The internal control algorithms in the autodriller and top drive must be able to realize the requested small changes in the setpoints corresponding to the excitation signals. This places a lower bound on the excitation signals' amplitudes, based on the resolution of these control systems.

There are several key parameters in the ES algorithm that need to be tuned. These parameters are the period (P) and amplitude (A) of the excitation signals (defined in Equations (7a), (7b) and (8)), as well as the adaptation rate (γ) and the tuning parameter k in Equations (11a) and (11b). These parameters should be tuned taking into account the guidelines presented in Table 1.

Table 1. Tuning considerations for key parameters in the ES algorithm.

Parameter	Tuning Considerations
Excitation amplitude, A	• Large enough to be realized by the autodriller and the top drive, as well as to cause a measurable response in the objective function through the *ROP*, *RPM*, *WOB* and torque. • Not too large, to avoid large disturbances to the overall process. • Scaled based on the planned range of *WOB* and *RPM* for the drilled section.
Excitation period, P	• Set $P_{wob} = 2P_{rpm}$ to minimize the interplay between the identified gradients with respect to *WOB* and *RPM* (see Appendix A). • Larger P_{wob} and P_{rpm} result in gradient estimates less sensitive to noise. • Trade-off between noise sensitivity and responsiveness to changes in drilling conditions
Adaptation rate, γ	• Larger γ results in faster convergence to the optimal *WOB* and *RPM* and higher responsiveness to changes in downhole drilling conditions. • Overly large γ makes the algorithm too sensitive to gradient estimation errors, e.g., when a formation shift occurs. • Trade-off between fast convergence and robustness.
k parameter	• As small as possible, yet leading to increase in *WOB* and *RPM* in the optimum zone (see Section 3.1.3)

4. Simulation Results

To simulate the dynamics of a control system on the rig that receives setpoints for *WOB* and *RPM* from the ES algorithm and steers the input variables to the requested setpoints as a function of time, the following functions were used to emulate this effect:

$$WOB(t) = WOB(t-1) + \frac{1}{\tau_{wob}}[WOB_{SP}(t-1) - WOB(t-1)], \tag{21a}$$

$$RPM(t) = RPM(t-1) + \frac{1}{\tau_{rpm}}[RPM_{SP}(t-1) - RPM(t-1)]. \tag{21b}$$

In Equations (21a) and (21b), the left-hand sides represent the current values of the *WOB* and *RPM* that are applied at the bit, while WOB_{SP} and RPM_{SP} are the corresponding setpoints. How quickly the control system is able to steer the *WOB* and *RPM* from their current values to new values dictated by the setpoints is determined by the time constants,

τ. For small values of τ, the *WOB* and *RPM* will quickly converge to their respective setpoints. For larger values of τ, convergence to the setpoints will take longer time.

The optimization algorithm and constraint handling approaches detailed in the previous sections were investigated by using the proposed extended model detailed in Equations (1)–(5) coupled with Equations (21a) and (21b) as a drilling simulator. In the simulation scenarios, the ES algorithm provides setpoints for the *WOB* and *RPM*, which are translated to applied *WOB* and *RPM* through Equations (21a) and (21b). The model simulates the *ROP* and torque response to these values of *WOB* and *RPM* that could be seen in the field for a given bit and formation. The current values for the *WOB*, *RPM*, *T* and *RPM* are "measured" from the extended model and used to calculate the *MSE* with Equation (6). These updated measurements are read by the ES algorithm and used to perform the optimization actions described in Section 3. It must be re-emphasized that the ES algorithm only uses measurements taken from the simulated drilling process to minimize the *MSE*, it has neither prior knowledge about the drilling model nor the locations of the different drilling dysfunctions.

The simulations emulate drilling in two generic formations, Formation *A* and Formation *B*. Formation *A* is described in detail in Section 2, where the optimal point to drill at in this lithology was identified to be at a *WOB* of 12,900 together with an *RPM* value of 89.5, as this combination minimizes the *MSE*. Formation *B* represents a softer formation than Formation *A*, otherwise they are identical. To emulate a preference for drilling with lower *WOB* and higher *RPM* in softer rocks, the onset of dysfunctions in Formation *B* are slightly different than in Formation *A*, placing the optimal point to drill at in Formation *B* at a *WOB* of 12,000 kg and an *RPM* value of 109. The parameters c_1, c_2, c_3 and c_4 that are used by the extended model in Equations (1) and (2) are provided in Table 2. These values are generated by picking generic values for the bit and formation parameters in the ranges suggested by Detournay et al. [28], and correspond to using units of kg for the *WOB*, rpm for the drill string rotational rate and the bit radius given in meters in Equations (1) and (2).

Table 2. Parameter values used in Equations (1) and (2).

Parameter	Fm. *A* Value	Fm. *B* Value	Units
c_1	1.4×10^{-6}	1.7×10^{-6}	$m^2/(kg{\cdot}rpm{\cdot}h)$
c_2	4.9×10^{-6}	5.9×10^{-6}	$m^2/(kg{\cdot}rpm{\cdot}h)$
c_3	3.05	3.05	m/s^2
c_4	7.01	7.01	m/s^2

All the simulation scenarios are initiated by ramping up the *WOB* and *RPM* to their starting setpoints, which is an initial guess at the optimal input values, which could e.g., be based on the driller's experience, a drill-off test, data from an offset well or estimates given by a drilling model. When the *WOB* and *RPM* have reached their initial values, the ES algorithm is activated and starts testing the drilling conditions with the excitation signals described by Equations (7a), (7b) and (8). After one full period of the *WOB* excitation signal, $P_{wob} = 120$ s, the buffers needed for the gradient estimation are filled up with the relevant measurements and the algorithm starts adapting the $\overline{WOB}$ and $\overline{RPM}$ in the direction that will reduce the *MSE*. The parameter values that are common in all the simulations are provided in Table 3.

Table 3. Parameter values that are common for all the simulations.

Parameter	Value	Units
D_{bit}	$12\ \frac{1}{4}$	Inches
γ_{wob}	2.5	kg/s
A_{wob}	200	kg
k_{wob}	0.001	MPa/kg
σ_{wob}	0.002	MPa/kg
P_{wob}	120	s
τ_{wob}	4	s
γ_{rpm}	0.02	rpm/s
A_{rpm}	2	rpm
k_{rpm}	0.05	MPa/rpm
σ_{rpm}	0.1	MPa/rpm
P_{rpm}	60	s
τ_{rpm}	3	s

4.1. Unconstrained Drilling Optimization

This section contains the results from two runs of simulated drilling through the homogeneous Formation *A*. The theoretical optimal point in this scenario is located approximately at a *WOB* of 12,900 kg in combination with an *RPM* value of 89.5. No constraints are considered in these two simulations, meaning that the ES algorithm is free to search for the drilling conditions that will minimize the *MSE* without any limits imposed on the torque or *ROP*.

Figure 10 shows the *WOB*, *RPM*, *MSE* and *ROP* for Simulation 1. The orange lines in the *WOB* and *RPM* tracks marks the base values, $\overline{WOB}$ and $\overline{RPM}$. This run was initiated with conservative values of 8000 kg *WOB* and 60 *RPM*, which resulted in drilling at a low *ROP* of about 11.5 m/h and a calculated *MSE* of approximately 184 MPa. After performing the initial variations in the input variables, the ES algorithm detects that increasing the *WOB* and *RPM* will result in more efficient drilling. Both the *WOB* and *RPM* are steadily increased by the algorithm until they converge to the region of the founder point after drilling for about 2700 s. The rest of the interval is drilled at peak efficiency, where the average *ROP* is 31.5 m/h, which is an increase of more than 170% from the starting point. Throughout the simulation, the *MSE* is only marginally reduced by the adaptation in the input variables. This is because the initial *WOB* and *RPM* from the start of the simulation resulted in dysfunction free phase II drilling, where the *MSE* was already close to its minimal value. The proposed ES algorithm is designed to interpret small or zero *MSE*-gradients as a situation where the corresponding input variable should be increased, which is why the $\overline{WOB}$ and $\overline{RPM}$ was adapted to the optimum in this scenario.

The values of $\overline{WOB}$ and $\overline{RPM}$ where the ES algorithm converges to in Simulation 1 are approximately 13,000 kg and 90 rpm, respectively, which are slightly higher than the pre-calculated values of 12,900 kg and 89.5 rpm. The ES algorithm's convergence to this point is caused by the *k* parameters used in Equation (11). The *k* values dictate that a (small) positive gradient must be calculated before the algorithm stops adaptation, and the point at which this occurs is slightly into the dysfunction region. This property can also be seen from Figures 4 and 5; the *MSE* does not significantly grow before the *WOB* and/or *RPM* has moved slightly into the dysfunction region, which is why the ES algorithm converges to the point seen in this simulation scenario.

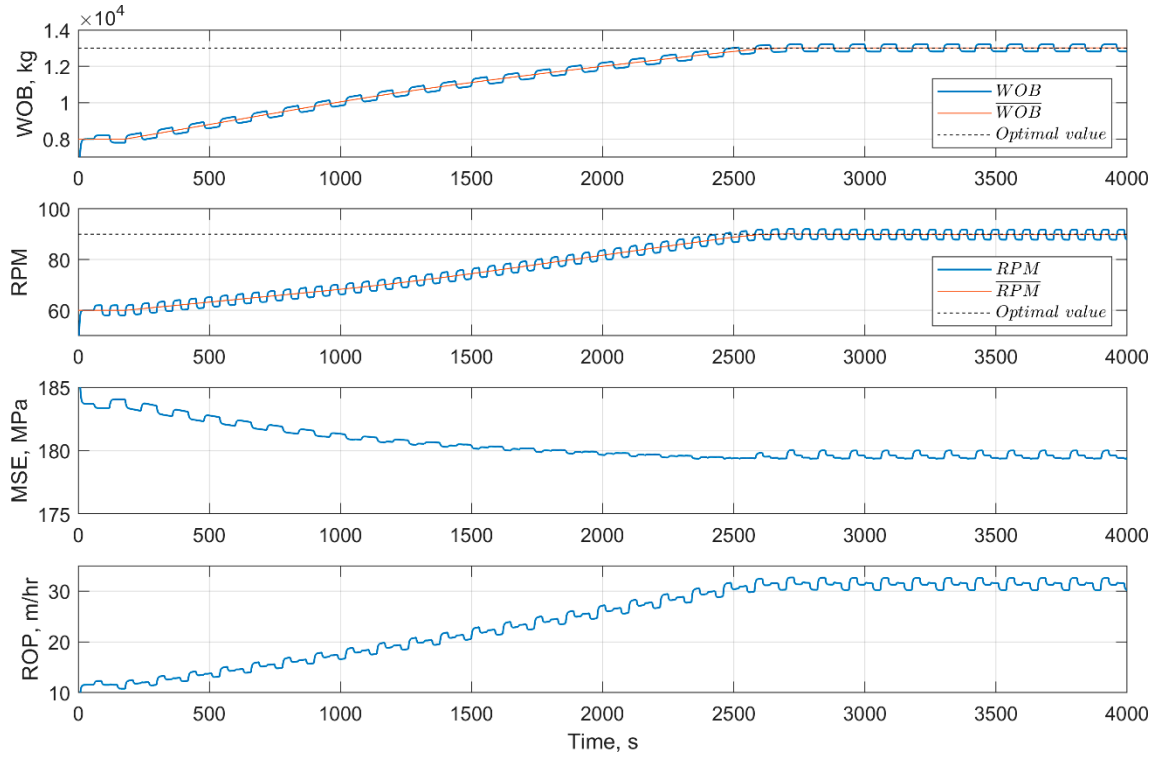

Figure 10. Simulation run 1, showing the ES algorithm converge to the optimum in the homogeneous formation *A*. The optimal *WOB* and *RPM* values indicated by the dotted lines are shown as an illustration and are not known by the ES algorithm.

Figure 11 shows the calculated gradients for Simulation 1, where it can be seen from the lower track that the estimated $\partial MSE/\partial RPM$ values show some oscillatory behavior until the *MSE* and *RPM* has converged to the optimum. This is caused by the adaptation in the *WOB* and *RPM* signals, which can sometimes interfere with accurate gradient estimation. A moving average of $\partial MSE/\partial RPM$ is plotted in the same track, which shows that the estimated gradient on average is unaffected by the oscillations. As long as the average gradients indicate which way the ES algorithm should adapt the input variables, the algorithm will be able to steer the *WOB* and *RPM* to the optimum. Figure 11 also shows the estimated gradients converging to a value equal to the k values for the respective signals, at which point the algorithm stops adjusting the $\overline{WOB}$ and $\overline{RPM}$.

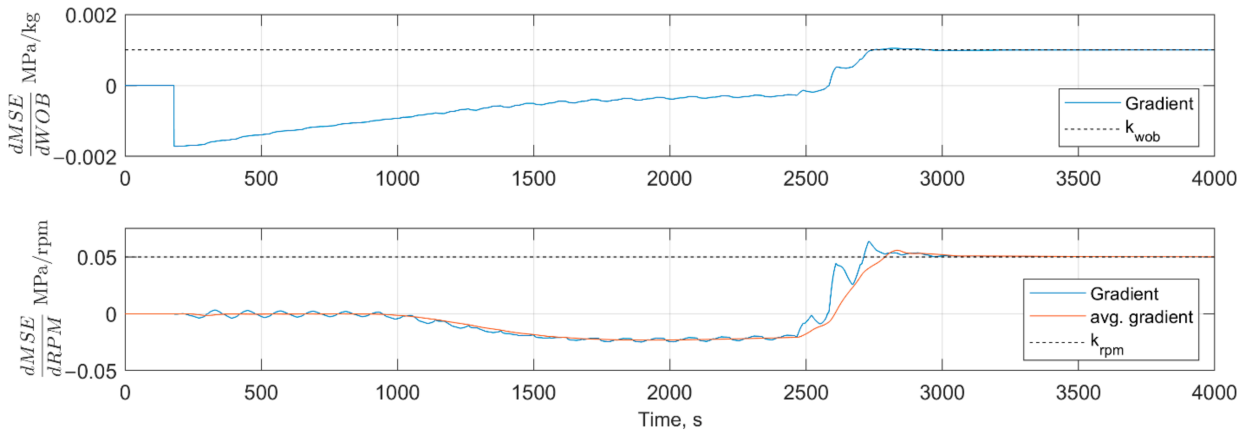

Figure 11. Estimated gradients in Simulation 1.

The results from Simulation 2 are displayed in Figure 12. This scenario is the same as Simulation 1, with the exception that the we initiate drilling at a *WOB* of 13,000 kg and with an *RPM* value of 160, which is in the dysfunction region (see Figure 2). The initial *WOB* is in fact the optimal *WOB* value, but only when combined with the appropriate *RPM*. As can be seen from Figure 12, drilling commences at a high average *MSE* value of about 300 MPa. The ES algorithm recognizes that we are drilling with a dysfunction and reduces both the *WOB* and *RPM* for the first 1800 s to exit the dysfunction region. At this point, the average *MSE* has been reduced to a value of approximately 181 MPa. As soon as the optimum zone is entered and it is safe to increase the *WOB* again, and the algorithm spends the next 3500 s converging more slowly to the optimal point. It can be noted that the adaptation in $\overline{WOB}$ and $\overline{RPM}$ that occurred during the first 1800 s happened at the algorithms maximal rate of 2.5 kg/s and 0.02 rpm/s, respectively. This is because of the large variations in *MSE* seen when drilling in the dysfunction region and the correspondingly large estimated gradients, which prompts the algorithm seek out better operating conditions as quickly as it is allowed to.

It can also be observed from Figure 12 that the adaptation that happens from 1800 s and onwards only results in small enhancements in *ROP* and *MSE*, the larger gains in drilling efficiency occurred during the early adaptation when moving out of the dysfunction region. At the start of the simulation, the *ROP* was about 33 m/h, which has been slightly reduced when compared to the *ROP* at the end of the run. The *MSE* has however been reduced substantially, which means that the drilling has become more energy efficient and possibly less detrimental for the bit and downhole tools.

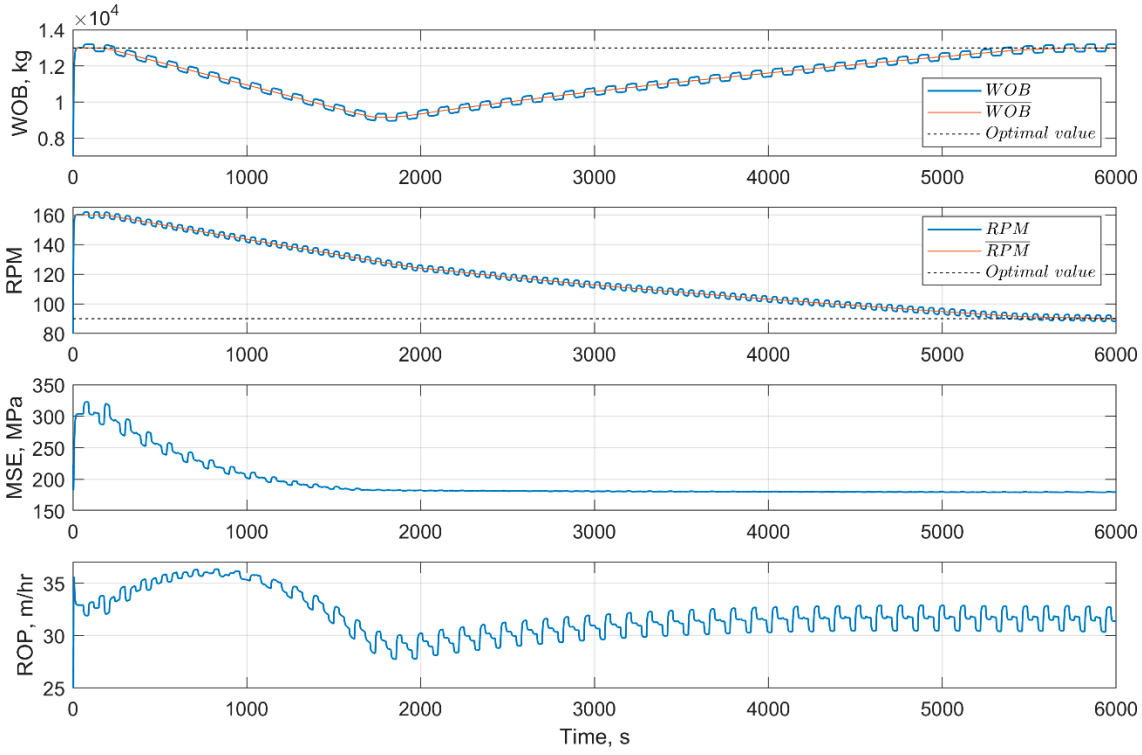

Figure 12. Simulation run 2, showing convergence for drilling initiated in the dysfunction region.

Figure 13 depicts the $\overline{WOB}$ and, $\overline{RPM}$ values from Simulations 1 and 2 in the *WOB*-*RPM* plane, together with contours which mark the *MSE* values for drilling in Formation *A*. The blue and orange datapoints can be viewed as the "path" that the ES algorithm took to converge to the founder point in these two scenarios. In the case of Simulation 2, it can be seen that the path taken by the algorithm is not the most efficient way to reach the founder point. It is however close to the most efficient path to exit the dysfunction region as quickly

as possible. Because of this "detour", more time is spent to converge to the optimum in Simulation 2, compared to Simulation 1.

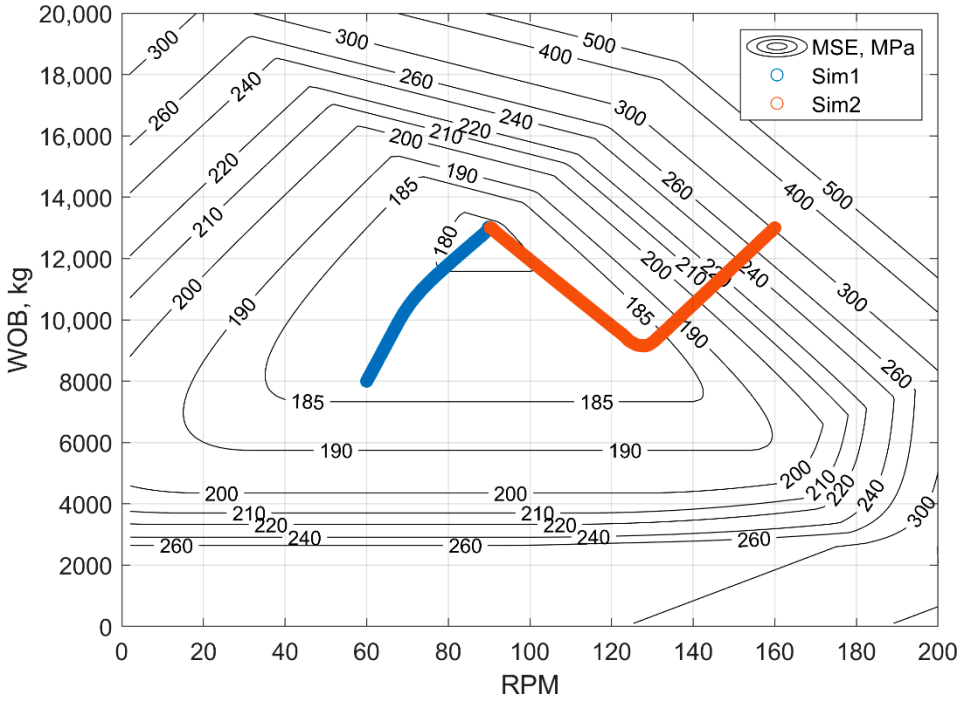

Figure 13. Contour plot of the *MSE* values for drilling in formation *A*, together with the $\overline{WOB}$ and $\overline{RPM}$ values for Simulations 1 and 2.

4.2. Constrained Drilling Optimization

In this section, the proposed constraint handling techniques are demonstrated in two simulation scenarios of drilling through the homogeneous formation *A*. In Simulation 3, we have imposed a maximal *ROP* of 20 m/h on the system through the use of Equation (13) with a ρ value of 0.1. This means that in this scenario, we seek to minimize the modified objective function given by Equation (13) and not the *MSE*. This run is initiated with the same values as in Simulation 1; a *WOB* of 8000 kg and an *RPM* value of 60. The results from Simulation 3 are shown in Figure 14, where it can be seen that the ES algorithm increases the applied *WOB* and *RPM* for the first 1300 s, before the *ROP* reaches the limiting value and the algorithm determines that any further adaptation will cause the *ROP* to exceed the allowable amount. Because of this constraint, the ES algorithm converges to the minimal *MSE* value that it can obtain while still drilling at an *ROP* at or below 20 m/h, which it finds at a *WOB* of 10,900 and an RPM of *71*. There are several operating points at which the ES algorithm could converge to in this scenario, based on the initial values for *WOB* and *RPM*. Because the MSE response in the optimal region is relatively constant, the algorithm will seek out the first combination of *WOB* and *RPM* that it can find that drills at the *ROP* limit. Any adaptation in the input variables beyond this operating point will cause the objective function to artificially grow through Equation (13), which will discourage any further changes to the *WOB* or *RPM* unless it significantly decreases the *MSE*.

In Simulation run 4, a maximal torque limit of 10,000 Nm is enforced by the predictive and reactive constraint handling approaches detailed in Equations (14) through (20). A safety factor of 2 is used in Equation (16), and the parameters K_P and K_I in Equation (18) have values of 0.05 kg/Nm and 0.001 kg/Nm·s, respectively. The initial setpoints for the *WOB* and *RPM* are 8000 kg and 100 rpm, respectively.

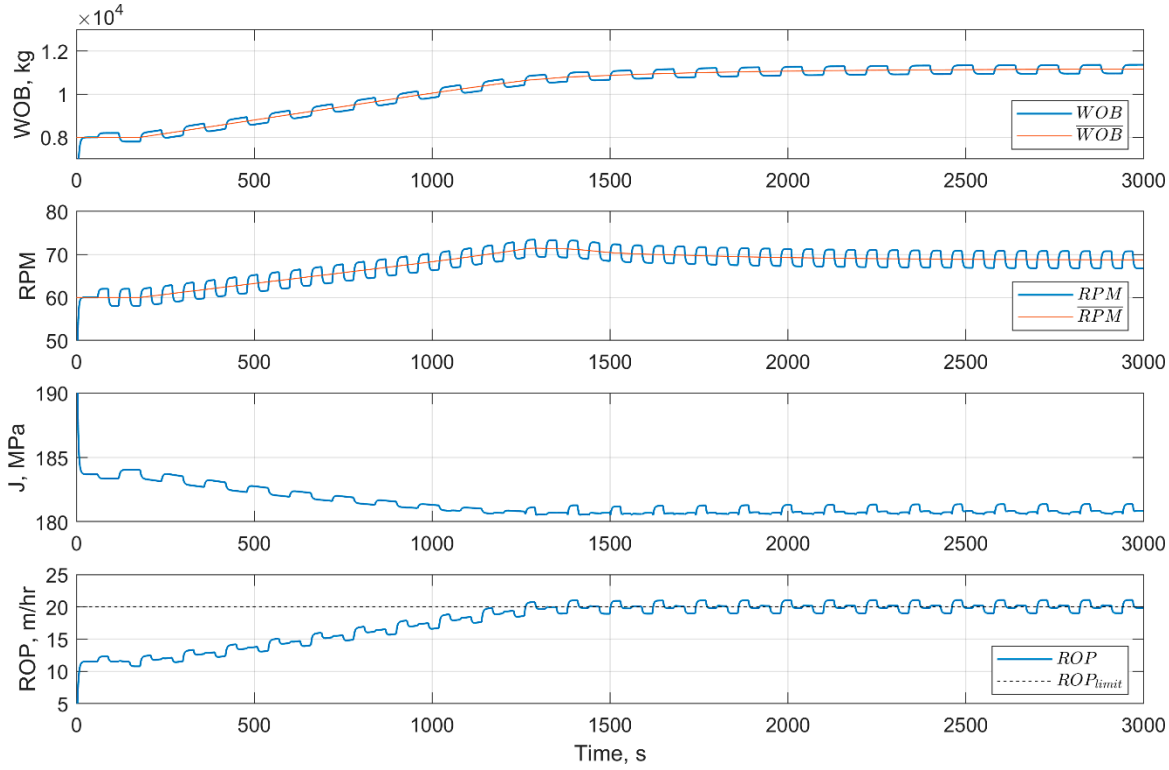

Figure 14. Simulation run 3, a scenario with a maximal limit imposed on the *ROP*.

Figure 15 displays the results from Simulation 4. In the first 1200 s, both the *WOB* and *RPM* are adapted to higher values, which results in drilling with lower *MSE* and higher *ROP*. At around 1200 s, Equation (16) predicts that the torque will surpass the allowable amount of 10,000 Nm if the *WOB* is increased any further. The adaptation in *WOB* is halted at this point and onwards, while the *RPM* continues to grow up to a value of approximately 111, where further increases in *RPM* would result in drilling in the dysfunction region. After 2000 s, an unexpected torque-increase of 1000 Nm is simulated, which makes the torque exceed its limit. This rise in torque could represent e.g., a build-up of cuttings around the BHA. As the torque is increased, the average *MSE* is elevated from about 180 to 200 MPa. The predictive constraint handler rapidly lowers the *WOB* until the torque is again within the allowable bounds, resulting in a reduction in $\overline{WOB}$ of about 900 kg. The reduction in $\overline{WOB}$ steers the drilling further away from the optimum, and the *MSE* is somewhat increased as a response. When drilling with this lower *WOB*, the ES algorithm detects that it is now safe to increase the *RPM* without encountering any dysfunctions which would increase the *MSE*. The *RPM* is seen to adapt to a value of 120, where the *ROP* is increased to approximately 29 m/h and we are drilling at the highest efficiency that can be obtained given the constraint on the torque.

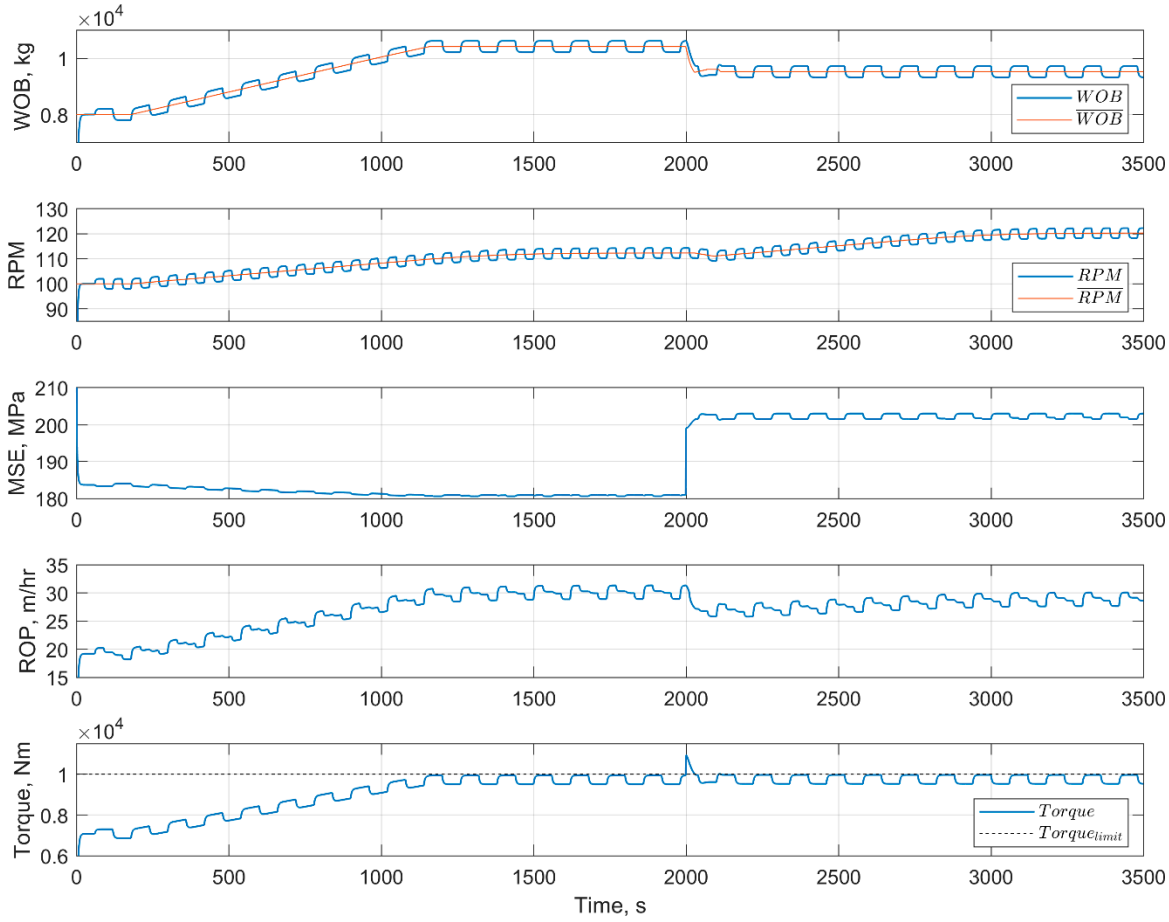

Figure 15. Simulation run 4, a scenario where the torque is not allowed to exceed 10,000 Nm.

4.3. Unconstrained Drilling with Formation Shifts

The results from Simulation 5 are shown in Figure 16, where we investigate how the proposed optimization algorithm handles abrupt formation changes. This scenario can be though as a continuation of Simulations 1 or 2, where the optimum for formation *A* was identified by the algorithm as 13,000 kg *WOB* and an *RPM* of 90. This scenario could also represent a setting where e.g., a drill-off test has been performed in formation *A*, which identified the optimal *WOB* and *RPM*. We initiate drilling with these optimal input values. After drilling 5 m in Formation *A*, we enter an 18-m-thick layer of the softer Formation *B*, at approximately 580 s. The optimal point in Formation *B* is located at a *WOB* of 12,000 kg and an *RPM* of 109, as indicated by the dotted lines in Figure 16. As we enter the softer formation, the *WOB* and *RPM* that were optimal for formation *A* are no longer the optimal input values to drill with and should be adjusted to drill more efficiently. Shortly after the formation shift occurs, the ES algorithm recognizes that the downhole conditions have changed and spends the following 1200 s converging to the optimal point in Formation *B*, where the *MSE* is minimized at an average value of 149 MPa and the average *ROP* has increased by approximately 20% from 36 to 43 m/h. At around 2200 s of simulation time, we enter Formation *A* again, and the *WOB* and *RPM* are slowly adjusted back to the optimal values that the simulation started out with. It can be seen that the "path" taken by the algorithm back to the optimum in Formation *A* consists of first reducing the $\overline{WOB}$ value before building it up to 13,000 kg, in the same manner as was done in Simulation 2 (see Figures 12 and 13) to quickly exit the dysfunction region.

Two important aspects of the proposed ES algorithm are shown in Figure 16. First, the advantage of continuously applying the excitations in *WOB* and *RPM* also even when we are operating at the current optimum, becomes apparent. When the drilled formation

suddenly changes, the information gathered by the excitation signals is used by the ES algorithm to rapidly recognize that the conditions have changed, and adjustments should be made in the applied $\overline{WOB}$ and $\overline{RPM}$ to drill more efficiently. These adjustments resulted in an increase in *ROP* of about 20%, compared to a setting where formation *B* had been drilled with constant *WOB* and *RPM* based on what was the optimal point when the simulation was initiated in formation *A*.

A second and closely related aspect is seen in the adjustments in $\overline{WOB}$,and $\overline{RPM}$ performed by the algorithm immediately after the formation change occurs at about 580 s of simulation time. In the following we consider the *WOB*, but the same analysis applies to the *RPM*. When the drilled formation becomes softer at 580 s, the calculated *MSE* is reduced. The ES algorithm relates this reduction in *MSE* to the currently applied *WOB*, which at this time was in an elevated position of $\overline{WOB} + A_{wob}$ kg. This causes the algorithm to estimate an artificially large and positive gradient for a short period of time, as higher values of *WOB* are related to a significant reduction in *MSE*. This erroneous gradient indicates that large improvements to the drilling efficiency can be made if $\overline{WOB}$ is increased. At this point, the adjustment of $\overline{WOB}$ in the wrong direction is limited by the saturation function and the adaptation gain in Equation (11), that disallows adaptation faster than 2.5 kg/s even if the estimated gradient is large. During the 50 s that the $\overline{WOB}$ is steered in the wrong direction, the $\overline{WOB}$ is only increased by about 125 kg. The requested changes in $\overline{WOB}$ would be much higher if the adaptation was directly proportional to the estimated gradient (as is usually the case in classical ES algorithms [26]). After drilling in this new formation for 50 s, the buffers used in the algorithm contain enough data sampled from the current conditions to detect that the $\overline{WOB}$ should be reduced to minimize the *MSE*, and the algorithm subsequently steers the $\overline{WOB}$ to the correct optimal value. The same effect as just described also occurs at the second formation shift at about 2200 s.

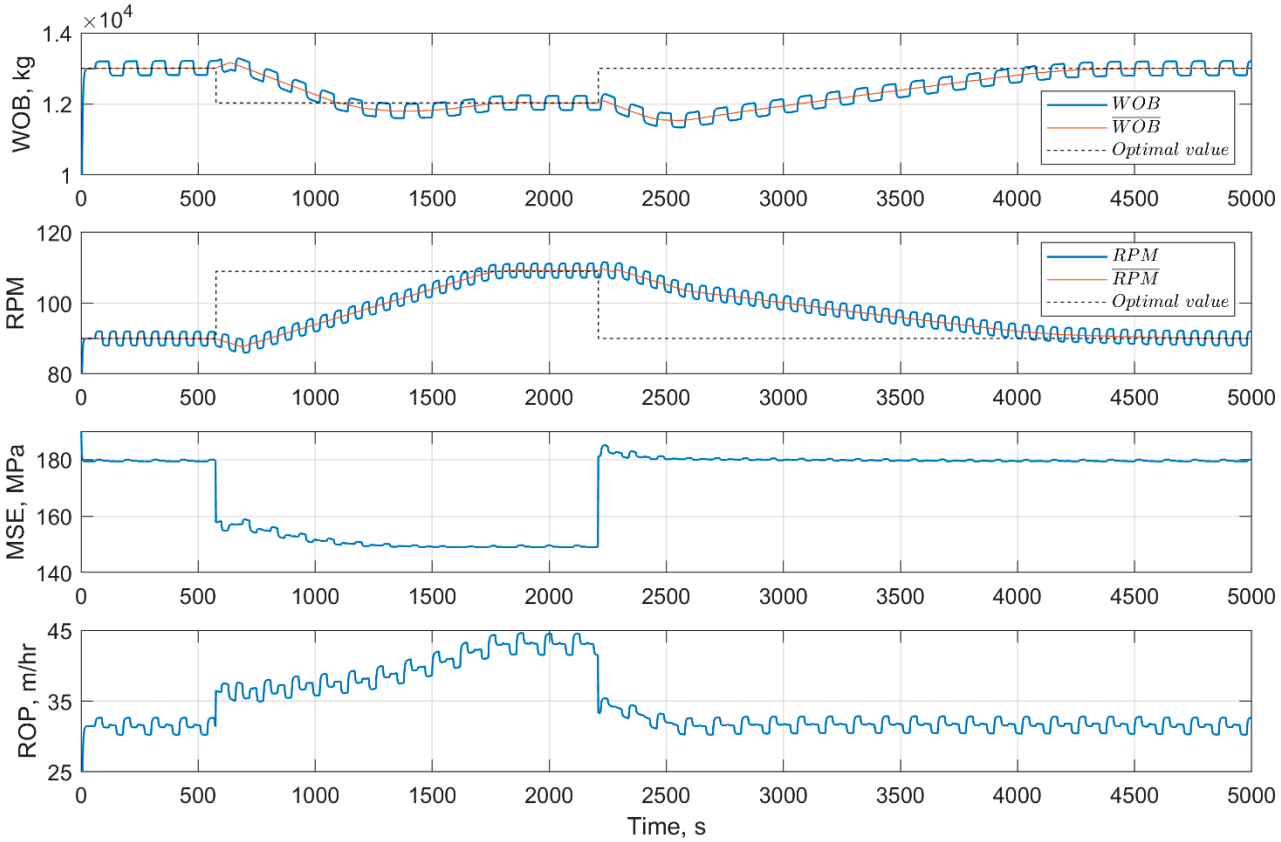

Figure 16. Simulation run 5, drilling through 5 m of formation *A*, 15 m of formation *B* and then returning to drilling in formation *A*.

5. Discussion of Results

The five simulation scenarios detailed in the previous section demonstrate how the proposed ES algorithm can be utilized to automatically steer the drilling process to the optimum conditions where the *MSE* is minimized. Since the optimization algorithm inherently requires full control of the *WOB* and *RPM* to continuously adjust these variables towards the optimal point, it is of utmost importance that the algorithm recognizes and avoids circumstances that could be damaging to the drilling equipment or could cause a contingency situation. In simulation 2 it was shown that the algorithm automatically steers away from drilling with dysfunctions, as drilling in this region resulted in high *MSE* values that could be reduced by regulating the *WOB* and *RPM*. In simulation runs 3 and 4, the possibly detrimental effects that we wish to avoid are not directly related to the *MSE*, but rather to other parameter that we wish to keep within certain limits. Simulations 3 and 4 demonstrate generic approaches to how we can avoid these types of constraints. In Simulation 4, the predictive constraint handling routine stops *WOB* adaptation before the constraint is violated. A separate control loop (the reactive constraint handling) is able to adjust the *WOB* back to the safe region when the limit is violated, much faster than if this constraint was implemented through modification of the objective function. This technique is however only applicable when the constrained output (the torque) is related to only one of the input variables, in this case the *WOB*. When several of the input variables are related to the output constraint, as is the case between the *WOB*, *RPM* and *ROP* in simulation run 3, the modified objective function described in Equation (13) is a better alternative to avoid the limit being exceeded.

The main advantage of using a data-driven algorithm like ES to optimize the drilling process is that it does not require detailed a priori knowledge of the downhole conditions or a drilling model to seek out more efficient drilling, and it can adapt to downhole changes. Both of these properties are shown in Simulation 5, where two formation shifts occurred which prompted the ES algorithm to seek out the new optimal conditions shortly after the changes happened. The ES algorithm considers a fixed window of time to perform its analysis and inherently tries to relate any change in the *MSE* to the applied excitations in *WOB* and *RPM*. If the *MSE* changes without any relation to the excitation signals, e.g., at a formation shift, the estimated gradients can become inaccurate when the data series used to estimate the gradients contain measurements from two differing downhole conditions. To avoid the algorithm having an exaggerated reaction to disturbances like this, the saturation function together with moderate values for the gain parameters, γ, is used to limit the algorithm's maximal adaptation rate regardless of the magnitude of the estimated gradients. This design encourages slow and steady adaptation towards the optimum. Faster convergence could be achieved by increasing γ, but this would also make the algorithm more susceptible to disturbances and noise.

Although the ES algorithm performs optimization actions without using a model of the system, engineering knowledge about the process is required to tune the algorithm and provide appropriate initial values for the *WOB* and *RPM*. In the simulation scenarios, the starting points were chosen to showcase different properties of the ES algorithm like constraint handling, convergence to the optimum and avoidance of drilling with dysfunctions. In simulation scenarios 1 and 5, the ES algorithm was able to increase the *ROP* by about 170% and 20%, respectively. How much the algorithm can improve the drilling efficiency (through higher *ROP* and/or lower *MSE*) is strongly related to how far away from the optimal *WOB* and *RPM* that the algorithm is initiated. In a field application, the initial *WOB* and *RPM* values should be a best guess of the optimal drilling conditions, which could be based on the driller's experience, a drill-off test, data from an offset well or estimates given by a drilling model.

There are both benefits and drawbacks to choosing *MSE* as the objective function to minimize. The *MSE* can be used to identify the founder point by seeking out the maximal *WOB* and *RPM* values that results in a decreasing or flat response in *MSE*. The expected flat region in *MSE* when operating in drilling region II can however pose some challenges

when applying the ES algorithm. When drilling in this region, the estimated gradients will have zero or near zero values and the ES algorithm depends on the parameters k_{wob} and k_{rpm} to indicate if the input variables should be increased. In field applications, the calculated *MSE* could be susceptible to noise (especially though the torque) which could make it hard to estimate zero or close to zero valued gradients. This complication could be alleviated by increasing the amplitudes and periods of the excitation signals or considering a longer sliding window time series that encompassed several oscillations of the excitation signals, which would average out disturbances. Another possible alternative could be to use a combination of *ROP* and *MSE* as the objective function, as in [25].

There are several paths for further research that could be explored. Additional studies on a more advanced drilling simulator, field trials or lab experiments are needed to investigate how dynamic effects such as vibrations affect the performance of the proposed algorithm. Tests in the field or in the lab would also provide the opportunity to compare the ES method with other optimization methods, either data-driven or model based, in a realistic setting. Testing the algorithm in e.g., a lab setting would allow us to study if the algorithm in its current form will be able to converge to the optimum if it is initiated in a region where severe vibrations occur. The extended model used to simulate drilling in this study assumes that the *MSE* will keep increasing when operating further into regions where vibrations are expected to occur (see Figures 4 and 5). If this is not the case, and the *MSE* rather reaches some plateau value that does not change as a function of *WOB* and *RPM* in these regions, the proposed ES algorithm would not be able to find the optimum if the initial point was in the *MSE* plateau region. If this is the case, a different objective function, e.g., on the form of Equation (13) could be used to remedy the issue.

A second possibility for further work relies on the ES method's inherent nature of relating measurements of drilling parameters to the known variations in *WOB* and *RPM* induced by the excitation signals. If available, additional measured and/or calculated parameters such as the magnitude of different forms of vibrations could be related to the variations in *WOB* and *RPM*. Knowing how downhole vibrations vary as a function of *WOB* and/or *RPM* could be utilized for constraint handling or be displayed as useful information for the driller.

6. Conclusions

We have presented an algorithm based on the multivariable extremum seeking method that automatically optimizes the WOB and RPM to achieve drilling with minimal MSE, while adhering to operational constraints for safe and efficient drilling. The algorithm detailed in the paper is data-driven and does not require detailed a priori knowledge or models of the drilling process. The algorithm gathers information about the current downhole conditions by continuously performing small tests with the applied WOB and RPM while drilling and automatically implements optimization actions based on the test results. To investigate the algorithm's performance in a simulation environment, a drilling model for bit-rock interaction has been extended by the authors to qualitatively account for drilling dysfunctions. The simulations demonstrate that the proposed algorithm is able to find and maintain the WOB and RPM that result in drilling with minimal MSE, while adhering to operational constraints. The constraint handling functionality has been demonstrated with limits imposed on the ROP and torque. Yet, it is generic and can be applied to other constraining factors. The simulations show that the ES method is able to track changes in the optimal WOB and RPM corresponding to changes in the drilled formation. As demonstrated in the simulation scenarios, the overall improvements in ROP can be up to 20–170%, depending on the initial guess of the optimal WOB and RPM obtained from e.g., a drill-off test or a potentially inaccurate model. Along with the algorithm's description, we provide an explanation of specific design choices and tuning guidelines that simplify the use of the algorithm in practice.

Author Contributions: Conceptualization, M.N., A.P. and B.S.A.; methodology, software, validation, formal analysis and writing—original draft preparation, M.N.; writing—review and editing M.N., A.P. and B.S.A.; visualization M.N., A.P. and B.S.A.; Supervision and project administration, A.P. and B.S.A. All authors have read and agreed to the published version of the manuscript.

Funding: This research was funded by the Norwegian University of Science and Technology through the BRU21 research program, www.ntnu.edu/bru21 (accessed on 25 February 2021).

Data Availability Statement: The simulation datasets and the Matlab code used in the model and simulations are available at: https://github.com/magnusnystad/Minimization-of-MSE-with-multivarable-ES (accessed on 25 February 2021).

Acknowledgments: This research is a part of BRU21—NTNU Research and Innovation Program on Digital and Automation Solutions for the Oil and Gas Industry, www.ntnu.edu/bru21 (accessed on 25 February 2021).

Conflicts of Interest: The authors declare no conflict of interest.

Abbreviations

BHA	Bottom Hole Assembly
ES	Extremum Seeking
MSE	Mechanical Specific Energy
NPT	Non-Productive Time
PDC	Polycrystalline Diamond Compact
PI	Proportional-Integral
RPM	Revolutions Per Minute (drill string rotational rate)
T	Torque
WOB	Weight on Bit

Appendix A. Period Selection for the Excitation Signals

The tuning of the excitation signals is an important part of the extremum seeking algorithm. To extract a gradient of how the *MSE* relates to the *WOB* and *RPM* independently, setting $P_{WOB} = 2P_{RPM}$ is suggested by the authors. Under some simplifying assumptions, it can be shown that this tuning of the excitation signal's periods allows for exact estimation of $\partial MSE/\partial WOB$ and $\partial MSE/\partial RPM$ without interference between the two excitation signals. Here, we investigate this property by considering the estimation of $\partial MSE/\partial WOB$ with a continuous-time, single-variable version of Equation (9), which is applied to a system where both the *WOB* and *RPM* is varied according to Equations (7a), (7b) and (8). A similar analysis can also be performed to show how the least-squares estimation of $\partial MSE/\partial RPM$ is not affected by the variations in the *WOB*.

Although the *MSE* is a non-linear function of both *WOB* and *RPM* when considering the entire span of *WOB* and *RPM* values (see Figures 4 and 5), the extremum seeking algorithm uses only a local region of this non-linear relationship when estimating gradients. The extent of this local region is determined by the amplitudes of the excitation signals. If suitable (not too large) amplitudes are used, it can be assumed that locally there is an approximately linear relationship between the *MSE* and the applied *WOB* and *RPM*, which is the relationship that is estimated by the least-squares gradient calculation in Equation (9). Using compact notation, let the *WOB* be denoted by $x = \overline{x} + d_x$ and the *RPM* be represented by $y = \overline{y} + d_y$, as detailed in Equations (7a) and (7b). In the neighborhood of the point $(\overline{x}, \overline{y})$, the non-linear relation between the *MSE*, *WOB* and *RPM* can be approximately described by:

$$z = \beta + \alpha xy, \tag{A1}$$

where z represents the MSE and the parameters α and β take on constant values in this local region. We further assume that the adaptation in *WOB* and *RPM* is small so that $\overline{x}$ and $\overline{y}$ are approximately constant throughout the investigated time interval of P_x seconds, as is common practice for average analysis of extremum seeking algorithms [26].

We consider a scenario where we are drilling ahead through a homogeneous formation and have varied the *WOB* (x) and *RPM* (y) according to Equation (8) while recording the *MSE* (z) for the past P_x seconds. The measured drilling data is used to solve for the least-squares slope and intercept parameters, a and b, using a continuous-time, single-variable version of Equation (9):

$$\int_{t-P_x}^{t} [z(\tau) - ax(\tau) - b]^2 d\tau \rightarrow \min_{a,b}, \tag{A2}$$

where a represents the gradient-estimate, $\partial MSE/\partial WOB$. Substituting in the previously defined relationships for x and y and approximating the response of the drilling system with Equation (A1) yields:

$$\int_{t-P_x}^{t} \left[\beta + \alpha\left(\overline{x}_y + d_x(\tau)\right)\left(\overline{y} + d_y(\tau)\right) - \alpha\left(\overline{x}_y + d_x(\tau)\right) - b\right]^2 d\tau \rightarrow \min_{a,b}. \tag{A3}$$

Further, using Equation (8) to describe the excitation signals, d_x and d_y, gives:

$$\int_{t-P_x}^{t} \left[\alpha + \beta\left(\overline{x} + A_x sgn\left(sin\left(\frac{2\pi\tau}{P_{xy}}\right)\right)\right)\left(\overline{y} + A_y sgn\left(sin\left(\frac{2\pi\tau}{P_y}\right)\right)\right) - a\left(\overline{x} + A_x sgn\left(sin\left(\frac{2\pi\tau}{P_{xy}}\right)\right)\right) - b\right]^2 d\tau \rightarrow \min_{a,b}. \tag{A4}$$

At any point in time, t, the integral in Equation (A4) can be split into intervals in which the signum function takes on constant values of ± 1. Using the relation $P_x = 2P_y$ and the assumption that $\overline{x}$ and $\overline{y}$ are constant values, Equation (A4) can be expressed as:

$$\min_{a,b}\left[P_x\left(\overline{x}_y^2 + A_x^2\right)\left(\alpha^2\overline{y}^2 + \alpha^2 A_y^2 - 2\alpha a\overline{y} + a^2\right) + 2P_x\overline{x}(\beta - b)(a - \alpha\overline{y}) + P_x(b - \beta)^2\right]. \tag{A5}$$

Taking the partial derivatives of Equation (A5) with respect to a and b and equating them to zero results in the set of equations:

$$\begin{gathered}(b - \beta) + \overline{x}(a - \alpha\overline{y}) = 0, \\ \left(x^2 + A_x^2\right)(a - \alpha\overline{y}) + 2\overline{x}(b - \beta) = 0,\end{gathered} \tag{A6}$$

which has the solution $a = \alpha\overline{y}$ and $b = \beta$. The estimated gradient, $\alpha\overline{y}$, corresponds to the slope of $\partial MSE/\partial WOB$ described by Equation (A1) evaluated at the average *RPM* value, $\overline{y}$. This shows that in an ideal scenario where the simplifying assumptions are met, the tuning $P_x = 2P_y$ allows for accurate estimation of $\partial MSE/\partial WOB$ without interference from the variations in *RPM*. The same analysis can be repeated for estimation of $\partial MSE/\partial RPM$ to find the expected gradient, $\alpha\overline{x}$, for this case. Other combinations of periods for the excitation signals can also be employed based on similar analysis, as long as one of the periods is an even multiple of the other, $P_{wob} = nP_{rpm}$ or $P_{rpm} = nP_{wob}$ where n is an even number larger than zero.

In reality, the applied *WOB* and *RPM* will exhibit dynamics and cannot be expected to perfectly follow the square wave setpoints requested by the extremum seeking algorithm. Any deviations from the setpoints will however be dealt with by the least-squares approach to gradient estimation, which will incorporate these transient periods into the analysis. Furthermore, if the system is not currently at the optimal point, there will be adaptation in both *WOB* and *RPM* which will make the base values, $\overline{x}$ and $\overline{y}$, change throughout the investigated time interval. The adaptation can cause some inaccuracies in the estimated gradients, but this effect can be kept to a minimum by choosing conservative values for the adaptation gains as well as through appropriate filtering of the data.

References

1. Eustes, A.W. The Evolution of Automation in Drilling. In Proceedings of the SPE Annual Technical Conference and Exhibition, Anaheim, CA, USA, 11–14 November 2007.
2. Chmela, B.; Gibson, N.; Abrahamsen, E.; Bergerud, R. Safer Tripping Through Drilling Automation. In Proceedings of the IADC/SPE Drilling Conference and Exhibition, Fort Worth, TX, USA, 4–6 March 2014.
3. Iversen, F.P.; Cayeux, E.; Dvergsnes, E.W.; Ervik, R.; Welmer, M.; Balov, M.K. Offshore Field Test of a New System for Model Integrated Closed-Loop Drilling Control. *SPE Drill. Completion* **2009**, *24*, 518–530. [CrossRef]
4. Gulsrud, T.O.; Nybø, R.; Bjørkevoll, K.S. Statistical Method for Detection of Poor Hole Cleaning and Stuck Pipe. In Proceedings of the SPE Offshore Europe Oil and Gas Conference and Exhibition, Aberdeen, UK, 8–11 September 2009.
5. Tarr, B.A.; Ladendorf, D.W.; Sanchez, D.; Milner, G.M. Next-Generation Kick Detection During Connections: Influx Detection at Pumps Stop (IDAPS) Software. *SPE Drill. Completion* **2016**, *31*, 250–260. [CrossRef]
6. Kyllingstad, A.; Nessjøen, P.J. A New Stick-Slip Prevention System. In Proceedings of the SPE/IADC Drilling Conference and Exhibition, Amsterdam, The Netherlands, 17–19 March 2009.
7. Runia, D.J.; Dwars, S.; Stulemeijer, I.P. A Brief History of the Shell "Soft Torque Rotary System" and Some Recent Case Studies. In Proceedings of the SPE/IADC Drilling Conference, Amsterdam, The Netherlands, 5–7 March 2013.
8. Chapman, C.D.; Sanchez, J.L.; De Leon Perez, R.; Yu, H. Automated Closed-Loop Drilling with ROP Optimization Algorithm Significantly Reduces Drilling Time and Improves Downhole Tool Reliability. In Proceedings of the IADC/SPE Drilling Conference and Exhibition, San Diego, CA, USA, 6–8 March 2012.
9. Dunlop, J.; Isangulov, R.; Aldred, W.D.; Sanchez, H.A.; Flores, J.L.S.; Herdoiza, J.A.; Belaskie, J.; Luppens, C. Increased Rate of Penetration Through Automation. In Proceedings of the SPE/IADC Drilling Conference and Exhibition, Amsterdam, The Netherlands, 1–3 March 2011.
10. Teale, R. The Concept of Specific Energy in Rock Drilling. *Int. J. Rock Mech. Min. Sci. Geomech. Abstr.* **1965**, *2*, 57–73. [CrossRef]
11. Koederitz, W.L.; Weis, J. A Real-Time Implementation of MSE. In Proceedings of the AADE National Technical Conference and Exhibition, Houston, TX, USA, 5–7 April 2005.
12. Dupriest, F.; Hutchison, I.; Oort, E.v.; Armstrong, N. *The IADC Drilling Manual—Drilling Practices*, 12th ed.; International Association of Drilling Contractors: Houston, TX, USA, 2014.
13. Dupriest, F.E.; Koederitz, W.L. Maximizing Drill Rates with Real-Time Surveillance of Mechanical Specific Energy. In Proceedings of the SPE/IADC Drilling Conference, Amsterdam, The Netherlands, 23–25 February 2005.
14. Wu, S.X.; Paez, L.; Partin, U.; Agnihotri, M. Decoupling Stick-Slip and Whirl to Achieve Breakthrough in Drilling Performance. In Proceedings of the IADC/SPE Drilling Conference and Exhibition, New Orleans, LA, USA, 2–4 February 2010.
15. Bataee, M.; Kamyab, M.; Ashena, R. Investigation of Various ROP Models and Optimization of Drilling Parameters for PDC and Roller-cone Bits in Shadegan Oil Field. In Proceedings of the International Oil and Gas Conference and Exhibition in China, Beijing, China, 8–10 June 2010.
16. Sui, D.; Aadnoy, B. Rate of Penetration Optimization using Moving Horizon Estimation. *Modeling Identif. Control A Nor. Res. Bull.* **2016**, *37*, 149–158. [CrossRef]
17. Young, F.S., Jr. Computerized Drilling Control. *J. Pet. Technol.* **1969**, *21*, 483–496. [CrossRef]
18. Rommetveit, R.; Bjørkevoll, K.S.; Halsey, G.W.; Larsen, H.F.; Merlo, A.; Nossaman, L.N.; Sweep, M.N.; Silseth, K.M.; Ødegaard, S.I. Drilltronics: An Integrated System for Real-Time Optimization of the Drilling Process. In Proceedings of the IADC/SPE Drilling Conference, Dallas, TX, USA, 2–4 March 2004.
19. Spencer, S.J.; Mazumdar, A.; Jiann-Cherng, S.; Foris, A.; Buerger, S.P. Estimation and Control for Efficient Autonomous Drilling Through Layered Materials. In Proceedings of the 2017 American Control Conference (ACC), Seattle, WA, USA, 24–26 May 2017; pp. 176–182.
20. Chang, D.-L.; Payette, G.S.; Pais, D.; Wang, L.; Bailey, J.R.; Mitchell, N.D. Field Trial Results of a Drilling Advisory System. In Proceedings of the International Petroleum Technology Conference, IPTC, Doha, Qatar, 19–22 January 2014.
21. Koederitz, W.L.; Johnson, W.E. Real-Time Optimization of Drilling Parameters by Autonomous Empirical Methods. In Proceedings of the SPE/IADC Drilling Conference and Exhibition, Amsterdam, The Netherlands, 1–3 March 2009.
22. Banks, S. Minimizing the Mechanical Specific Energy While Drilling Using Extremum Seeking Control. In Proceedings of the 11th International Conference on Vibration Problems, Lisbon, Portugal, 9–12 September 2013.
23. Aarsnes, U.J.F.; Aamo, O.M.; Krstic, M. Extremum Seeking for Real-time Optimal Drilling Control. In Proceedings of the American Control Conference (ACC), Philadelphia, PA, USA, 10–12 July 2019.
24. Nystad, M.; Pavlov, A. Micro-Testing While Drilling for Rate of Penetration Optimization. In Proceedings of the International Conference on Offshore Mechanics and Arctic Engineering, Virtual, Online, 3–7 August 2020.
25. Lai, S.W.; Ng, J.; Eddy, A.; Khromov, S.; Paslawski, D.; van Beurden, R.; Olesen, L.; Payette, G.S.; Spivey, B.J. Large-Scale Deployment of a Closed-Loop Drilling Optimization System: Implementation and Field Results. *SPE Drill. Completion* **2020**. [CrossRef]
26. Tan, Y.; Moase, W.H.; Manzie, C.; Nešić, D.; Mareels, I.M. Extremum seeking from 1922 to 2010. In Proceedings of the 29th Chinese Control Conference, Beijing, China, 29–31 July 2010.
27. Sui, D.; Nybø, R.; Azizi, V. Real-time optimization of rate of penetration during drilling operation. In Proceedings of the 2013 10th IEEE International Conference on Control and Automation (ICCA), Hangzhou, China, 12–14 June 2013; pp. 357–362.

28. Detournay, E.; Richard, T.; Shepherd, M. Drilling response of drag bits: Theory and experiment. *Int. J. Rock Mech. Min. Sci.* **2008**, *45*, 1347–1360. [CrossRef]
29. Vogel, S.K.; Creegan, A.P. Case Study for Real Time Stick/Slip Mitigation to Improve Drilling Performance. In Proceedings of the SPE/IADC Middle East Drilling Technology Conference and Exhibition, Abu Dhabi, United Arab Emirates, 26–28 January 2016.
30. Warren, T.M. Penetration Rate Performance of Roller Cone Bits. *SPE Drill. Eng.* **1987**, *2*, 9–18. [CrossRef]
31. Dupriest, F.E. Comprehensive Drill Rate Management Process To Maximize ROP. In Proceedings of the SPE Annual Technical Conference and Exhibition, San Antonio, TX, USA, 24–27 September 2006.
32. Pessier, R.C.; Fear, M.J. Quantifying Common Drilling Problems With Mechanical Specific Energy and a Bit-Specific Coefficient of Sliding Friction. In Proceedings of the SPE Annual Technical Conference and Exhibition, Washington, DC, USA, 4–7 October 1992.
33. Dupriest, F.E.; Witt, J.W.; Remmert, S.M. Maximizing ROP With Real-Time Analysis of Digital Data and MSE. In Proceedings of the International Petroleum Technology Conference, Doha, Qatar, 21–23 November 2005.
34. Simon, R. Energy Balance in Rock Drilling. *Soc. Pet. Eng. J.* **1963**, *3*, 298–306. [CrossRef]
35. Oloruntobi, O.; Butt, S. Application of specific energy for lithology identification. *J. Pet. Sci. Eng.* **2020**, *184*. [CrossRef]
36. Menand, S.; Mills, K. Use of Mechanical Specific Energy Calculation in Real-Time to Better Detect Vibrations and Bit Wear While Drilling. In Proceedings of the AADE National Technical Conference and Exhibition, Houston, TX, USA, 11–12 April 2017.
37. Yau, H.-T.; Lin, C.-J.; Wu, C.-H. Sliding Mode Extremum Seeking Control Scheme Based on PSO for Maximum Power Point Tracking in Photovoltaic Systems. *Int. J. Photoenergy* **2013**, *2013*. [CrossRef]
38. Ariyur, K.B.; Krstić, M. *Real-Time Optimization by Extremum Seeking Control*; John Wiley & Sons, Inc.: Hoboken, NJ, USA, 2003. [CrossRef]
39. Tan, Y.; Nešić, D.; Mareels, I. On the Choice of Dither in Extremum Seeking Systems: A Case Study. *Automatica* **2008**, *44*, 1446–1450. [CrossRef]
40. Payette, G.S.; Spivey, B.J.; Wang, L.; Bailey, J.R.; Sanderson, D.; Kong, R.; Pawson, M.; Eddy, A. A Real-Time Well-Site Based Surveillance and Optimization Platform for Drilling: Technology, Basic Workflows and Field Results. In Proceedings of the SPE/IADC Drilling Conference and Exhibition, The Hague, The Netherlands, 14–16 March 2017.